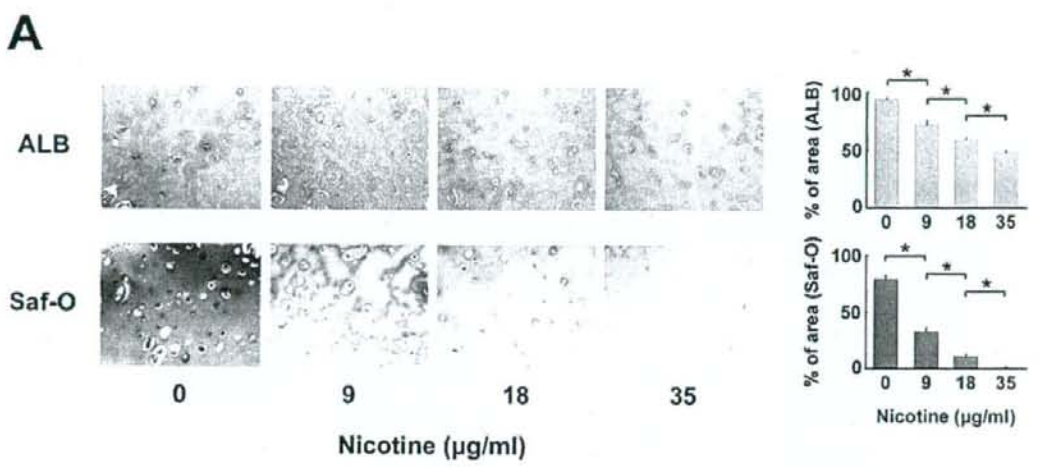

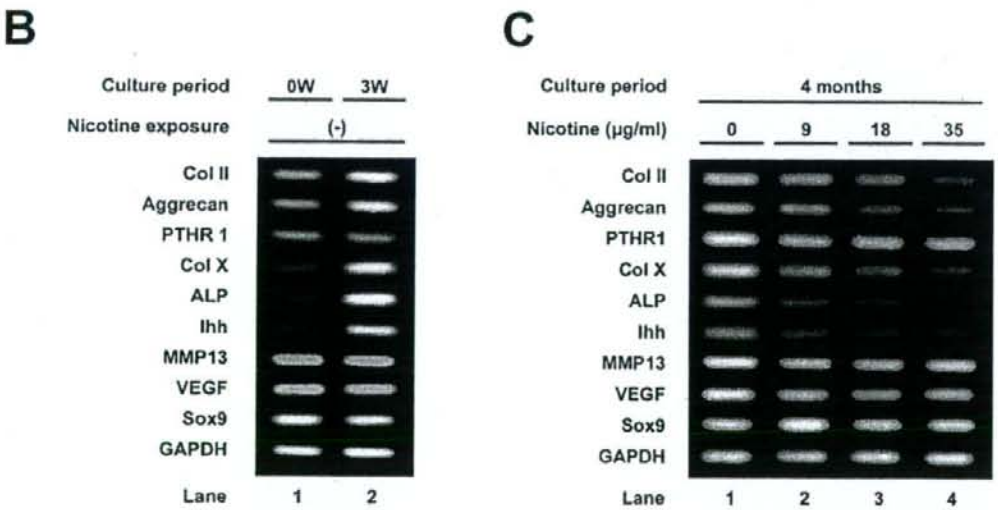

Figure 3. Long-term (four months) effect of nicotine on growth plate chondrocytes in alginate beads. Growth plate chondrocytes in alginate beads were exposed to the indicated concentration of nicotine for four months. A: Microscopic view of chondrocytes in alginate beads after four-months cultivation. Upper panels: ALB stain, lower panels: Safranin-O stain. Chondrocytes were surrounded by matrix which they secreted. Nicotine decreased the area stained with ALB or Safranin-O in a concentration-dependent manner. *, statistically significant, $P<0.02$. B: RT-PCR analysis of chondrocyte-specific gene expression in the chondrocytes at the start of cultivation (lane 1: 0W) and three weeks (lane 2: 3W). From top to bottom: genes for Col II, Aggrecan, parathyroid hormone receptor type 1 (PTHR1), Col X, alkaline phosphatase (ALP), Indian hedgehog (Ihh), matrix metalloproteinase type13 (MMP13), vascular endothelial growth factor (VEGF), Sox9 and GAPDH. C: RT-PCR analysis of chondrocyte-specific gene expression in chondrocytes embedded in alginate beads exposed to the indicated concentration of nicotine for four months. Expression of early stage matrix-gene (Col II and Aggrecan) and markers of hypertrophic chondrocytes (Col X, ALP and Ihh) increased after three weeks of cultivation (B). Nicotine decreased the expression of these genes in a concentration-dependent manner, but had little effect for the expression of MMP13, VEGF, and control genes (Sox9 and GAPDH) (C).
doi:10.1371/journal.pone.0003945.g003

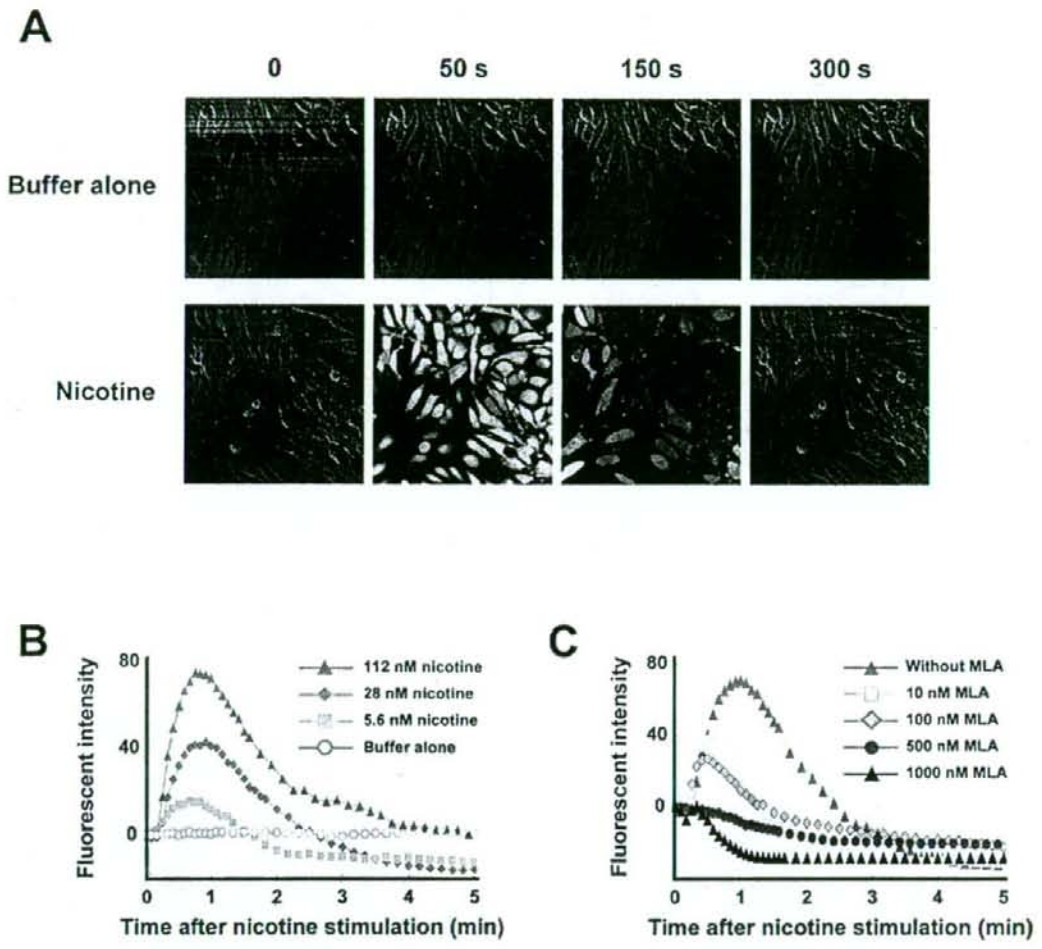

Figure 4. Calcium influx assay in primary chondrocyte culture. Nicotine-stimulated calcium signaling was investigated by the use of a fluorescent Ca^{2+} indicator. Primary chondrocyte cultures were stimulated by nicotine with or without MLA, the specific antagonist of alpha7 homomeric nAChR. A: Addition of assay buffer alone elicits no reaction (upper panels: negative control). Nicotine elicits a transient increase of intracellular calcium (lower panels). B: Nicotine elicits a transient increase of intra-cellular calcium in a concentration-dependent manner. C: MLA inhibits nicotine-induced calcium influx in a concentration-dependent manner. The cells were treated with MLA 30 min before nicotine stimulation.
doi:10.1371/journal.pone.0003945.g004

(Figure 6C). Besides, scatterplot and correlation between the FL and the BW revealed that nicotine downwardly shifted the linear slope in alpha7 nAChR +/+ fetuses but had no effect in alpha7 nAChR −/− fetuses (Figure 6D). These findings suggest that maternal nicotine exposure decreased the fetal endochondral ossification through the fetal alpha7 nAChR in vivo.

Discussion

Alpha7 nAChR was originally identified as a subunit of neuronal nAChR, and has also been shown to be functional in both neuronal and non-neuronal, i.e., non-excitable cells such as lymphocytes, vascular endothelial cells, keratinocytes and bronchial epithelium [16]. In this study, we demonstrated the expression of the alpha7 subunit of nAChR at resting to pre-hypertrophic chondrocytes in murine growth plate and on a culture of human growth plate chondrocytes, and the involvement of alpha7 nAChR in nicotine-induced delayed skeletal growth. The novel findings of alpha7 nAChR in chondrocytes suggest that the effect of smoking on delayed skeletal growth is directly correlated with nicotinic action on chondrocytes.

Direct effect of nicotine on human growth plate chondrocytes

Maternal nicotine exposure decreases the width of the hypertrophic zone of growth plate, increases apoptotic chondrocytes, and reduces the length of femur in rat [20]. Contrarily, nicotine has been shown to up-regulate glycosaminoglycan and

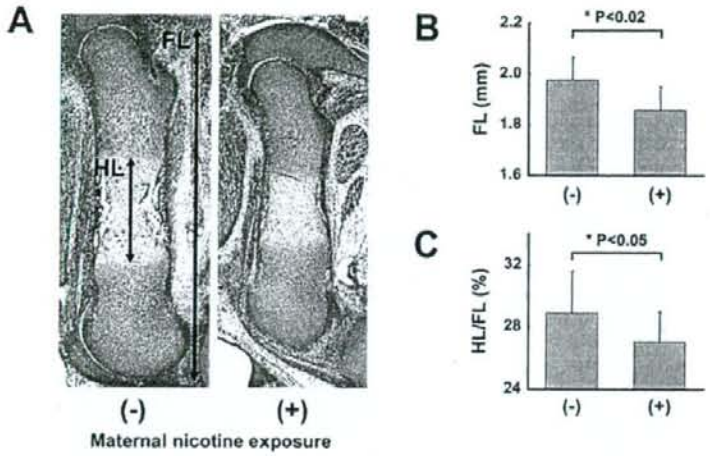

Figure 5. Maternal nicotine exposure in wild-type mice. Ovulation-induced pregnant mice were mated and were given drinking water with nicotine during pregnancy. At noon on gestational day 15, the fetuses were sacrificed, and their legs were histologically investigated. A: Skeletal growth estimated by measuring the femur length (FL) and the length of the hypertrophic zone of the femur (HL). B: FL (mm), C: HL/FL (%) of E15.5 fetuses whose mothers were given drinking water with or without nicotine. Nicotine significantly decreased FL and HL/FL.
doi:10.1371/journal.pone.0003945.g005

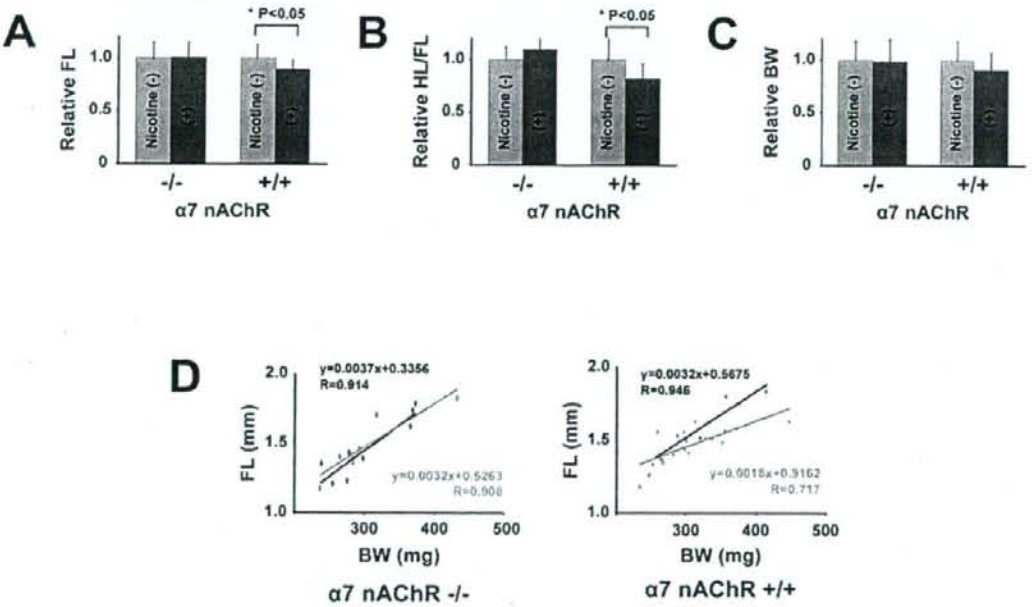

Figure 6. Maternal nicotine exposure in alpha7 nAChR-disrupted mice. A–C: FL, HL/FL, and body weight (BW) of alpha7 nAChR −/− and alpha7 nAChR +/+ E15.5 littermate fetuses. Alpha7 nAChR +/− female were mated with alpha7 nAChR +/− male, and given drinking water with or without nicotine during pregnancy. Relative FL, HL/FL, and BW were calculated, each value in mice that did not receive nicotine was regarded as equal to 1.0. Nicotine significantly reduced FL and HL/FL in alpha7 nAChR +/+ fetuses but not in alpha7 nAChR −/− fetuses (A,B). Nicotine did not significantly reduce BW in either genotype (C). D: Scatterplot and correlation between the FL and BW of mice with (red line) or without (black line) exposure to nicotine. In alpha7 nAChR +/+ fetus, Nicotine downwardly shifts the linear slope in alpha7 nAChR +/+ fetuses but not in alpha7 nAChR −/− fetuses.
doi:10.1371/journal.pone.0003945.g006

collagen synthesis of human articular chondrocytes in vitro [21]. Cultured human growth plate chondrocytes derived from infant fingers serve as a good model for analyzing whether nicotine has direct action on growth plate chondrocytes. The present findings of nicotinic effect, i.e. decreasing matrix synthesis and suppressing hypertrophic differentiation but not proliferation on growth plate chondrocytes in vitro, indicate the direct effect of nicotine on growth plate chondrocytes. The findings are consistent with reports that maternal nicotine exposure has a negative effect on endochondral ossification in animals [13]. Besides, these findings are consistent, considering the fact that longitudinal skeletal growth is partly caused by matrix synthesis and hypertrophic differentiation of chondrocytes. Confirmation of the animal model using "human" chondrocytes is essential since certain chemicals, such as thalidomide, exhibit different effects in humans and rodents.

Differences of expression levels of the genes for Col X, ALP, Ihh, MMP13, and VEGF in alginate beads culture (Figure 3B, C) may attribute to differential regulation among hypertrophic markers. Expression of the Ihh, Col X, and ALP genes were down-regulated by nicotine and the MMP13 and VEGF genes remained unaffected. Alternatively, the difference could be a result of chondrocyte culture, that is, artifactual induction ex vivo, and the MMP13 and VEGF genes were indeed expressed at the start of alginate bead culture with chondrocytes at passage 1 (Fig. 3B, lane 1: "0 W"). In contrast, the Col X, ALP, and Ihh genes were appropriately regulated after three-dimensional culture (Figure 3B, lane 2: "3 W"; Figure 3C, lane 1: without exposure to nicotine), as is the case with gene regulation in the growth plate.

Involvement of alpha7 nAChR in delayed endochondral ossification

The alpha7 nAChR-null mice exhibit normal development, including neural tissue, but alpha7 nAChR-null mice lack nicotinic currents in hippocampal neurons [22], and show abnormalities in late-stage keratinocyte development in the epidermis [23]. Lack of phenotypic abnormality in the femur of fetuses (Figure 5B) and adults indicates that ACh signaling through alpha7 nAChR has little involvement in the process of physiological skeletal growth. Results using MLA, the antagonist to alpha7 nAChR, strongly suggest the involvement of alpha7 nAChR in the nicotinic effect on chondrocytes. Such low-molecular weight substances may, however, have additional unclarified action in addition to any "specific" action. The proof of alpha7 nAChR involvement in delayed skeletal growth was strengthened by the in vivo experiments with alpha7 nAChR gene-disrupted mice. Especially so, considering the fact that maternal nicotine exposure caused delayed skeletal growth in only alpha7 nAChR +/+ fetuses compared with their alpha7 nAChR −/− littermates, fetal alpha7 nAChR but not maternal alpha7 nAChR is responsible for the mechanism of nicotine-induced delayed skeletal growth.

Since nicotine exposure has been reported to be epidemiologically and experimentally correlated with maternal effect, i.e., abnormal placental function and blood flow [10], the physiological and pathological function of alpha7 nAChR in growth plate was confirmed by comparing "littermates" of alpha7 nAChR (Figure 6B). This comparison confirms involvement of alpha7 nAChR on the fetus, and eliminates a possibility of maternal effect. Furthermore, decrease of relative femur length (Figure 6C, scatterplot and correlation, right panel, alpha7 nAChR +/+) and lack of nicotinic effect on body weight of alpha7 nAChR fetuses (Figure 6B, right panel, "BW") by maternal nicotine exposure indicate a specific effect of nicotine on bone growth rather than a systemic effect. Therefore, the effect of smoking during pregnancy on skeletal growth may be attributed to this direct action of nicotine on growth plate chondrocytes, at least in part.

Our studies suggest that, from the large number of chemicals associated with cigarette smoking, nicotine may cause delayed skeletal growth and, indeed, amniotic fluid and breast milk both have higher concentrations of nicotine than maternal serum does [24]. In addition, metabolism of nicotine in the fetus and child is much slower than that in adults [25]. We therefore should pay close attention to the effect of smoking, regardless of being active or passive, on growth plate chondrocytes. This nicotinic effect may also extend to the delay of fracture repair or generation of non-union in adults, since the process of bone repair also partly depends on endochondral ossification.

Materials and Methods

Chondrocyte cultures

Human chondrocytes were isolated from epiphysis of extra fingers, which were surgically excised from patients with polydactyly. Ethical approval for tissue collection was granted by the Institutional Review Board of the National Research Institute for Child Health and Development, Tokyo, Japan (#88). Minced tissue was incubated for 1 h at 37°C in 0.08% trypsin in PBS, then for 6 h at 37°C in 0.2% collagenase type 1 (Wako, Osaka, Japan) in Dulbecco's Modified Eagle's medium (DMEM). The released cells were washed and resuspended in DMEM containing 10% fetal bovine serum (FBS, Sanko Junyaku Co., Tokyo, Japan, lot number: 27110307) and plated at a density of 1×10^6 cells per 100 mm dish for primary monolayer cultures, or 1×10^5 cells per 35 mm dish for calcium influx assay and immunocytochemical assay of nAChR. In each experiment, we used one lot of cultured chondrocytes from extra fingers obtained from four patients.

RT-PCR for detection of nAChR subunit

Total RNA was prepared from epiphysis of extra fingers using Isogen (Nippon Gene) according to the manufacturer's recommendations. DNase-treated RNA was reverse transcribed in 20 µl of RT-PCR mix (50 mM Tris, pH 8.3, 3 mM $MgCl_2$, 75 mM KCl, 50 mM dNTPs, 2.5 µM oligo$(dT)_{20}$, 5 mM DTT, 2 U RNaseOUT and 10 U SuperScriptIII (Invitrogen) at 50°C for 1 h. The PCR was performed in a final volume of 50 µl containing 1 µl of the single strand cDNA product, 25 mM TAPS (pH 9.3), 50 mM KCl, 2.0 mM $MgCl_2$, 1 mM β-mercaptoethanol , 200 µM dNTPs, and AmpliTaq Gold (Applied Biosystems) and 20 pmol of each forward (5′) and reverse (3′) primers (Table S1). For each experiment the housekeeping gene GAPDH was amplified with 25–35 cycles to normalize the cDNA content of the samples. The amplification was performed for 30 cycles, with other conditions following polymerase-producing manufacturer's recommendations. Human brain and skeletal muscle RNAs were purchased from Ambion (Austin, TX).

Western blot analysis for detection of nAChR subunit

Total proteins were isolated from primary monolayer cultures using CelLyticTM-M Mammalian Cell Lysis/Extraction Reagent (Sigma). The proteins were separated by SDS-PAGE (Bio-Rad) in a 10% acrylamide gel, then blotted at 60 V for 2 h at 4°C onto a nitrocellulose membrane. Non-specific binding was blocked by incubation in TBS containing 10% BSA and 0.05% Tween-20. The membrane was subsequently incubated at 4°C overnight with the monoclonal antibody to nicotinic acetylcholine receptor, alpha7 subunit (Sigma, St-Louis, MO; product number: N 8158) diluted 1:3000. After rinsing, the membrane was incubated for 1 h at room temperature in horseradish peroxidase-conjugated rabbit

anti-rat IgG antibody (Sigma; A 5795) at a dilution of 1:3000 in TBS containing 0.05% Tween-20. After rinsing, the membrane was immersed in ECL solution (GE Healthcare, Buckinghamshire, UK). Then, the blots were visualized by LAS-1000plus IDX2, the luminescent image analyzer (Fuji Photo Film, Japan).

Immunocytochemical and immunohistochemical analysis

Immunocytochemical analysis was performed as previously described [26]. Briefly, dishes were incubated with antibody to alpha7 subunit of nAChR in PBS containing 1% BSA. As a methodological control, the primary antibody was omitted. After washing in PBS, dishes were incubated with horseradish peroxidase (HRP)-conjugated rabbit anti-rat IgG antibody. Staining was developed by using a solution containing diaminobenzidine and 0.01% H_2O_2 in 0.05 M Tris-HCl buffer, pH 6.7.

For immunohistochemical analysis, hind legs of E15.5 C57BL/6J mice were prepared, fixed in 4% paraformaldehyde phosphate buffer solution (Wako) overnight at 4°C, and embedded in paraffin. Immunohistochemical analysis was performed as previously described [27]. Briefly, slides were treated with 0.4% pepsin (DAKO) at 37°C for 30 min, incubated with primary antibody to alpha7 subunit of nAChR(Sigma, product number: N 8158) diluted 1:2000 in PBS containing 1% BSA at room temperature for 3 h, and incubated with simple mouse stain MAX-PO (RAT), a second antibody, at room temperature for 1 h. Staining was developed by using a solution containing diaminobenzidine and 0.01% H_2O_2 in 0.05 M Tris-HCl buffer, pH 6.7. Finally, slides were counterstained with hematoxylin.

Agarose gel cultures

Chondrocytes were cultured in agarose-stabilized suspension using a modified method as previously described [28]. Primary monolayer cultures were trypsinized, re-suspended in agarose gel medium : DMEM/F-12 containing 10% FBS, 100 units/ml penicillin G, 100 mg/ml streptomycin, and 50 mg/ml ascorbate, to a concentration of 2×10^4 cells/ml, then mixed with equal volume of 1% low-temperature melting agarose (Sigma-Aldrich, Steinheim, Germany) in agarose gel medium, giving a final concentration of 1×10^4 cells/ml suspended in 0.5% low-temperature melting agarose in agarose gel medium (suspension agarose). Three milliliters of suspension agarose were added to 60 mm culture plates that were precoated with 2 ml of 1% autoclaved standard agarose (Bio-Rad, Hercules, CA). The gel was allowed to solidify at 4°C before addition of agarose gel medium. Then, culture plates were placed in a 37°C, 5% CO_2 humidified incubator for 21 days, and medium containing indicated concentration of nicotine was replaced once at the beginning of the week. After 21 days, suspension agarose was transferred to a glass slide, and placed on a plate warmer at 50°C with a covering of positively-charged nylon membranes (Roche, Mannheim, Germany). The slides were completely dried in a incubator at 42°C overnight, and fixed in 4% paraformaldehyde for 15 min, and stained with ALB to identify colonies producing glycosaminoglycans and to observe histologically. Colonies were defined as a cluster of cells with a diameter greater than 50 μm. ALP activity was determined in non-fixed agarose slide by Histofine, ALP substrate kit (Nichirei, Tokyo, Japan) following the manufacturer's product information. Type 10 collagen expression was also determined in the agarose slide using specific monoclonal antibody (Sigma; product number: C7974). The slide was fixed in acetone (Nacalai Tesque, Kyoto, Japan) at room temperature for 20 min. Non-specific binding was blocked with 2.5% normal rabbit serum (DakoCytomation, Glostrup, Denmark) in PBS containing 1% BSA and 1% Triton X-100. Slides were incubated for 6 h at room temperature with primary antibody, diluted 1:2000 in PBS containing 1% BSA. Bound antibody was detected by HRP-conjugated polyclonal rabbit anti-mouse IgM antibody (Dako, Glostrup, Denmark; product number: P 0260) diluted 1:100 in PBS at room temperature for 30 min. Peroxidase activity was visualized with diaminobenzidine tetrahidrochloride plus 0.03% H_2O_2, and slide was counterstained with hematoxylin.

Alginate bead cultures

Chondrocytes were cultured in alginate beads following the method described by De Ceuninck et al. Primary monolayer cultures were trypsinized, washed, and centrifuged. The isolated chondrocytes were suspended at a concentration of 2×10^6 cells/ml in a 1.25% alginate in 0.15 M NaCl. The cell suspension was slowly expressed through a 21 gauge needle and dropped into a 102 mM $CaCl_2$ solution. The beads with approximately 25,000 cells/bead were allowed to polymerize for 10 min and washed three times with 0.15 M NaCl, followed by two washes in DMEM/F12. The beads were then transferred to medium (200 beads/10 ml/60 mm culture dish): DMEM/F-12 containing 10% FBS, 50 μg/ml ascorbate, 100 units/ml penicillin G, 100 mg/ml streptomycin. The beads were cultured at 37°C in a 5% CO_2 humidified incubator for four months, and medium with or without nicotine was replaced twice weekly. The beads were transferred to new dishes every other week to avoid the formation of monolayer cultures on the bottom of the dish by chondrocytes escaping from the beads.

For histological analysis, the beads were fixed in 4% paraformaldehyde, 0.1 M cacodylate buffer, pH 7.4, containing 10 mM $CaCl_2$ for 4 h at room temperature, and then washed overnight at 4°C in 0.1 M cacodylate buffer, pH 7.4, containing 50 mM $BaCl_2$. The beads were dehydrated through alcohols and embedded in paraffin. The sections were routinely stained with ALB and safranin-O.

For RT-PCR analysis, chondrocytes were separated from the beads by incubating the beads in dissolution solution (at a ratio of 200 μl/bead), containing 55 mM EDTA, for 5 min and centrifuged. Total RNA was isolated by using RNeasy (Qiagen) following manufacturer's instructions, and was converted to cDNA by same method as described above. The sequences of PCR primers of human chondrocyte-related gene are listed in Table S2. PCR was performed in a final volume of 50 μl containing 2 μl of the single strand cDNA product (10 ng/μl), 10 mM Tris-HCl (pH8.3), 50 mM KCl, 1.5 mM $MgCl_2$, 200 μM dNTPs, 1.25 U Taq (Takara), and 20 pmol of each forward (5′) and reverse (3′) primers.

Calcium imaging

Primary monolayer cultures in 35 mm glass-bottomed plates were prepared. At near confluence, measurement was done by using Fluo-4 NW calcium assay kit (Molecular Probes, product number: F36206) following the manufacturer's product information. In short, the cells were incubated in dye loading solution containing 2.5 mM probenecid at 37°C for 30 min, then at room temperature for an additional 30 min before nicotine stimulation. The fluorescence was measured in LSM 510 (Carl Zeiss) with the settings appropriate for argon laser. Nicotine and its antagonists were prepared as a solution in assay buffer. If antagonists were used, they were added 30 min prior to nicotine stimulation.

Maternal nicotine exposure in wild-type mice

Three-month-old pregnant mice were purchased at day 1 of pregnancy from Sankyo Laboratories (Tokyo, Japan). The mice were given drinking water containing 2% sucrose (Wako, Osaka, Japan) with or without nicotine (hydrogen tartrate salt; Sigma-

Aldrich, St. Louis, MO). Nicotine was added to the sucrose solution starting at an initial concentration of 25 μg/ml to the treatment group mice. This was increased to 50 μg/ml on days 3 to 4, 100 μg/ml after day 5. The control mice were given only sucrose solution as a drinking water. The pregnant mice were sacrificed at noon on gestational day 15. The embryo were immediately weighed, and the legs were immediately removed and fixed in 4% paraformaldehyde phosphate buffer solution (Wako) for 24 h. Then, the legs were dehydrated through alcohols, embedded in paraffin, and sections were stained with Hematoxylin and Eosin for histological analysis.

Maternal nicotine exposure in alpha7 nAChR-disrupted mice

B6.129S7-Chrna7<tm1Bay>/J, the alpha7 nAChR +/− mice were obtained from Charles River Laboratories Japan. Ten- to 12-week old alpha7 nAChR +/− mice were mated, and pregnant mice were given sucrose solution with or without nicotine. The fetuses were obtained and analyzed as in the case of wild-type C57BL/6J mice, as described above. The alpha7 nAChR genotype was determined by means of PCR reaction with the specific primers (Table S3).

Statistics

The results of the quantative assays were expressed as mean±S.D. Significance was determined with Student's *t* test and ANOVA. All experiments were replicated twice.

Supporting Information

Figure S1 In vivo chondrocytic proliferation assay. A: Paraffin section of the femur of E15.5 C57BL/6J mice immunohistochemically stained with antibody to PCNA. Proliferative chondrocytes extensively stained positive for PCNA regardless of maternal nicotine exposure. B: Percentage of PCNA-positive cells in chondrocytes of the proliferative zone. There is no significant difference between the two groups. Hind legs of E15.5 C57BL/6J mice were prepared, fixed in 4% paraformaldehyde phosphate buffer solution (Wako) overnight at 4°C, and embedded in paraffin. After deparaffinization, slides were autoclaved in 0.01 M citrate buffer (pH 6.0) for 10 min, incubated with primary antibody to PCNA (DAKO: PC10) diluted 1:400 in PBS containing 1% BSA at room temperature for 3 h, and incubated with polyclonal rabbit anti-mouse immunoglobrins/HRP (DAKO: P260) at room temperature for 1 h. Staining was undertaken using a solution containing diaminobenzidine and 0.01% H_2O_2 in 0.05 M Tris-HCl buffer at pH 6.7, followed by counterstaining with hematoxylin.
Found at: doi:10.1371/journal.pone.0003945.s001 (0.06 MB PDF)

Table S1 Primers for nAChR subunit genes
Found at: doi:10.1371/journal.pone.0003945.s002 (0.03 MB PDF)

Table S2 Primers for chondrocyte specific genes
Found at: doi:10.1371/journal.pone.0003945.s003 (0.01 MB PDF)

Table S3 Primers for genotypying alpha7 nAChR gene
Found at: doi:10.1371/journal.pone.0003945.s004 (0.01 MB PDF)

Acknowledgments

We would like to express our sincere thanks to M. Nasu, C-H. Cui, H. Akutsu, K. Miyado, and M. Toyoda for support throughout this work, to H. Abe for providing expert technical assistance, to K. Saito and Y. Ito for their secretarial work, and to A. Crump for reviewing the manuscript.

Author Contributions

Conceived and designed the experiments: AK AU. Performed the experiments: AK HM. Analyzed the data: AK HM AU. Contributed reagents/materials/analysis tools: KS HI ST YT. Wrote the paper: AK AU.

References

1. Davies DP, Abernethy M (1976) Cigarette smoking in pregnancy: Associations with maternal weight gain and fetal growth. Lancet 1: 385–387.
2. Hardy JB, Mellits ED (1972) Does maternal smoking during pregnancy have a long-term effect on the child? Lancet 2: 1332–1336.
3. Wingerd J, Schoen EJ (1974) Factors influencing length at birth and height at five years. Pediatrics 53: 737–741.
4. Karatza AA, Varvarigou A, Beratis NG (2003) Growth up to 2 years in relationship to maternal smoking during pregnancy. Clin Pediatr (Phila) 42: 533–541.
5. Sexton M, Hebel JR (1984) A clinical trial of change in maternal smoking and its effect on birth weight. Jama 251: 911–915.
6. Yerushalmy J (1971) The relationship of parents' cigarette smoking to outcome of pregnancy–implications as to the problem of inferring causation from observed associations. Am J Epidemiol 93: 443–456.
7. Olsen J, Pereira Ada C, Olsen SF (1991) Does maternal tobacco smoking modify the effect of alcohol on fetal growth? Am J Public Health 81: 69–73.
8. Trygg K, Lund-Larsen K, Sandstad B, Hoffman HJ, Jacobsen G, et al. (1995) Do pregnant smokers eat differently from pregnant non-smokers? Paediatr Perinat Epidemiol 9: 307–319.
9. Haddon W Jr, Nesbitt RE, Garcia R (1961) Smoking and pregnancy: carbon monoxide in blood during gestation and at term. Obstet Gynecol 18: 262–267.
10. Mochizuki M, Maruo T, Masuko K (1985) Mechanism of foetal growth retardation caused by smoking during pregnancy. Acta Physiol Hung 65: 295–304.
11. Nordstrom ML, Cnattingius S (1996) Effects on birthweights of maternal education, socio-economic status, and work-related characteristics. Scand J Soc Med 24: 55–61.
12. Mau G (1976) Letter: Smoking and the fetus. Lancet 1: 972.
13. Nelson E, Jodscheit K, Guo Y (1999) Maternal passive smoking during pregnancy and fetal developmental toxicity. Part 1: gross morphological effects. Hum Exp Toxicol 18: 252–256.
14. El-Zawawy HB, Gill CS, Wright RW, Sandell LJ (2006) Smoking delays chondrogenesis in a mouse model of closed tibial fracture healing. J Orthop Res 24: 2150–2158.
15. Olsen J (1992) Cigarette smoking in pregnancy and fetal growth. Does the type of tobacco play a role? Int J Epidemiol 21: 279–284.
16. Sharma G, Vijayaraghavan S (2002) Nicotinic receptor signaling in nonexcitable cells. J Neurobiol 53: 524–534.
17. Arneric SP, Brioni JD (1999) Neuronal nicotinic receptors : pharmacology and therapeutic opportunities. New York: Wiley-Liss, xii, 421 p.
18. Tacchetti C, Quarto R, Nitsch L, Hartmann DJ, Cancedda R (1987) In vitro morphogenesis of chick embryo hypertrophic cartilage. J Cell Biol 105: 999–1006.
19. Hauselmann HJ, Fernandes RJ, Mok SS, Schmid TM, Block JA, et al. (1994) Phenotypic stability of bovine articular chondrocytes after long-term culture in alginate beads. J Cell Sci 107 (Pt1): 17–27.
20. Kurtoglu S, Gunes T, Koklu E, Bastug O, Canoz O, et al. (2007) Influence of maternal nicotine exposure on neonatal rat bone: protective effect of pentoxifylline. Exp Biol Med (Maywood) 232: 398–405.
21. Guillahorn L, Lippiello L, Karpman R (2005) Smoking and osteoarthritis: differential effect of nicotine on human chondrocyte glycosaminoglycan and collagen synthesis. Osteoarthritis Cartilage 13: 942–943.
22. Orr-Urtreger A, Goldner FM, Saeki M, Lorenzo I, Goldberg L, et al. (1997) Mice deficient in the alpha7 neuronal nicotinic acetylcholine receptor lack alpha-bungarotoxin binding sites and hippocampal fast nicotinic currents. J Neurosci 17: 9165–9171.
23. Arredondo J, Nguyen VT, Chernyavsky AI, Bercovich D, Orr-Urtreger A, et al. (2002) Central role of alpha7 nicotinic receptor in differentiation of the stratified squamous epithelium. J Cell Biol 159: 325–336.
24. Luck W, Nau H, Hansen R, Steldinger R (1985) Extent of nicotine and cotinine transfer to the human fetus, placenta and amniotic fluid of smoking mothers. Dev Pharmacol Ther 8: 384–395.

25. Dempsey D, Jacob P 3rd, Benowitz NL (2000) Nicotine metabolism and elimination kinetics in newborns. Clin Pharmacol Ther 67: 458–465.
26. Sano M, Umezawa A, Abe H, Akatsuka A, Nonaka S, et al. (2001) EAT/mcl-1 expression in the human embryonal carcinoma cells undergoing differentiation or apoptosis. Exp Cell Res 266: 114–125.
27. Sano M, Umezawa A, Suzuki A, Shimoda K, Fukuma M, et al. (2000) Involvement of EAT/mcl-1, an anti-apoptotic bcl-2-related gene, in murine embryogenesis and human development. Exp Cell Res 259: 127–139.
28. Benya PD, Shaffer JD (1982) Dedifferentiated chondrocytes reexpress the differentiated collagen phenotype when cultured in agarose gels. Cell 30: 215–224.

OPEN ACCESS Freely available online PLoS one

Human Sclera Maintains Common Characteristics with Cartilage throughout Evolution

Yuko Seko[1,2], Noriyuki Azuma[2], Yoriko Takahashi[1], Hatsune Makino[1], Toshiyuki Morito[3], Takeshi Muneta[3], Kenji Matsumoto[4], Hirohisa Saito[4], Ichiro Sekiya[5], Akihiro Umezawa[1]*

1 Department of Reproductive Biology and Pathology, National Institute for Child and Health Development, Tokyo, Japan, 2 Department of Ophthalmology, National Center for Child Health and Development, Tokyo, Japan, 3 Section of Orthopaedic Surgery, Tokyo Medical and Dental University, Tokyo, Japan, 4 Department of Allergy and Immunology, National Institute for Child and Health Development, Tokyo, Japan, 5 Section of Cartilage Regeneration, Tokyo Medical and Dental University, Tokyo, Japan

Abstract

Background: The sclera maintains and protects the eye ball, which receives visual inputs. Although the sclera does not contribute significantly to visual perception, scleral diseases such as refractory scleritis, scleral perforation and pathological myopia are considered incurable or difficult to cure. The aim of this study is to identify characteristics of the human sclera as one of the connective tissues derived from the neural crest and mesoderm.

Methodology/Principal Findings: We have demonstrated microarray data of cultured human infant scleral cells. Hierarchical clustering was performed to group scleral cells and other mesenchymal cells into subcategories. Hierarchical clustering analysis showed similarity between scleral cells and auricular cartilage-derived cells. Cultured micromasses of scleral cells exposed to TGF-βs and BMP2 produced an abundant matrix. The expression of cartilage-associated genes, such as Indian hedge hog, type X collagen, and MMP13, was up-regulated within 3 weeks in vitro. These results suggest that human 'sclera'-derived cells can be considered chondrocytes when cultured ex vivo.

Conclusions/Significance: Our present study shows a chondrogenic potential of human sclera. Interestingly, the sclera of certain vertebrates, such as birds and fish, is composed of hyaline cartilage. Although the human sclera is not a cartilaginous tissue, the human sclera maintains chondrogenic potential throughout evolution. In addition, our findings directly explain an enigma that the sclera and the joint cartilage are common targets of inflammatory cells in rheumatic arthritis. The present global gene expression database will contribute to the clarification of the pathogenesis of developmental diseases such as high myopia.

Citation: Seko Y, Azuma N, Takahashi Y, Makino H, Morito T, et al. (2008) Human Sclera Maintains Common Characteristics with Cartilage throughout Evolution. PLoS ONE 3(11): e3709. doi:10.1371/journal.pone.0003709

Editor: Che John Connon, University of Reading, United Kingdom

Received July 31, 2008; **Accepted** October 8, 2008; **Published** November 12, 2008

Funding: This study was supported by Research Fellowships of the Japan Society for the Promotion of Science (JSPS) for Young Scientists; a grant from the Ministry of Education, Culture, Sports, Science and Technology (MEXT) of Japan and Health and Labor Sciences Research Grants; by a Research grant on Health Science Focusing on Drug Innovation from the Japan Health Science Foundation; by the Program for Promotion of Fundamental Studies in Health Science of the Pharmaceuticals and Medical Devices Agency; by a grant from the Terumo Life Science Foundation; by a Research Grant for Cardiovascular Disease from the Ministry of Health, Labor and Welfare; and by a Grant for Child Health and Development from the Ministry of Health, Labor and Welfare.

Competing Interests: The authors have declared that no competing interests exist.

* E-mail: umezawa@1985.jukuin.keio.ac.jp

Introduction

The eye receives information from the outside as the retinal image, converting it into electrical signals for the brain, leading to visual perception. The retinal image is stabilized by the balance of intraocular pressure and the curvatures of the scleral and corneal envelope. In order to keep this balance, the rigidity of the sclera and the cornea are essential, especially the sclera must be rigid enough for the eyeball to be rotated by powerful extraocular muscles adhering to the sclera. The sclera and the corneal stroma that are anatomically continuous have common characteristics such as mechanical rigidity, and share a common origin, i.e., the neural crest. However, the cornea and the sclera are different in transparency: the cornea is completely transparent to produce a sharp image on the retina; the sclera is opaque to avoid the internal light scattering affecting the retinal image. This corneal transparency has been attributed to significant changes in the structure, especially of collagen fibrils, in the latter stages of development [1]. Multipotent progenitor/precursor cells of corneal stroma are identified from the mouse eye [2]. On the other hand, existence of multipotent progenitor/precursor cells in the sclera remains unclarified. Although the sclera does not contribute significantly to visual perception, scleral diseases such as refractory scleritis, scleral perforation and pathological myopia are considered incurable or difficult to cure.

Microarray analysis of murine scleral development [3] and global sequencing analysis from the human scleral cDNA library [4] have been reported. To clarify pathogenesis of developmental diseases such as high myopia, a database of genes expressed in the sclera of younger donors is important. We here demonstrate with a global expression database of human infant sclera that the sclera derived from the neural crest evolutionarily retains characteristics of cartilage.

Results

Isolation and cell culture of human scleral cells

Scleral tissues were excised from surgical specimens collected during treatment for retinoblastoma. The scleral tissue was cut into smaller pieces and cultured in the growth medium. The scleral cells began growing out almost one week after the start of cultivation. Scleral cells exhibited a fibroblast-like spindle shape or polygonal shape in morphology when cultured in monolayer (Fig. 1A). The cells from PD 5 to PD 31 rapidly proliferated in culture, and propagated continuously (Fig. 1B). The cells stopped replicating and became broad and flat at PD 43 or 264 days, indicating that they had entered senescence. The morphological changes are PD-dependent.

Global outlook by hierarchical clustering and PCA

To clarify the specific gene expression profile of scleral cells, we compared the expression levels of 54,675 probes in the cultured scleral cells and other cultured cells (Table 1) using the Affymetrix GeneChip oligonucleotide arrays. We first performed hierarchical clustering and PCA on the expression pattern. PCA showed similarity between scleral cells and chondrocytes derived from elastic cartilage (Fig. 2A). Hierarchical clustering analysis based on all probes showed similarity between scleral cells and chondrocytes (Fig. 2B). This similarity led us to hypothesize that the scleral cells are chondrocytes when proliferated ex vivo, or have a chondrogenic potential. We then performed PCA from the expression data of cartilage-associated genes, including aggrecan, Sox9, and parathyroid hormone receptor (Table S1). These genes are categorized as "cartilage condensation" or "proteoglycan biosynthesis" according to Gene Ontology. PCA based on cartilage-associated genes demonstrated that scleral cells are grouped into the same category that includes chondrocytes, synovial cells, and synovial fluid-derived cells (Fig. 2C). The synovial cells and synovial fluid-derived cells used in this study have a strong chondrogenic potential [5–7]. Hierarchical clustering analysis based on the cartilage-associated genes also demonstrated that sclera, cartilage, synovium, and joint fluid are categorized into the same group (Fig. 2D, Fig. 2E, Fig. S1).

Table 1. Human cells analyzed in this study.

Title	Description
Bone marrow	Bone marrow-derived cell (P1)
Hepatocyte	Hepatocyte (P0)
Endometrium	Endometrial cell
Synovium	Synovium-derived cell (P1)
Joint fluid	Joint fluid-derived cell (P1)
Muscle	Muscle-derived cell (P1)
Bone	Cancellous bone-derived cell (P1)
Fat	Subcutaneus fat-derived cell (P1)
Amniotic epithelium	Amniotic epithelial cell (P4)
Umbilical cord (1)	Umbilical cord-derived cell (P0) (1)
Umbilical cord (2)	Umbilical cord-derived cell (P0) (2)
Cartilage	Auricular cartilage-derived cell (P1)
Sclera	Sclera-derived cell (P1)
Cornea (stroma)	Keratocyte (P1)
Periostium	Periostium-derived cell (P1)
Dermis	Dermal fibroblast (P2)
Cortical bone	Cortical bone-derived cell (P3)

Gene chip analysis was performed using RNAs from the cells obtained from each tissue. The cells obtained from bone marrow, liver, synovium, joint fluid, muscle, bone, and fat were cultivated as previously described [31–33]. Amniotic epithelial cells and umbilical cord-derived cells were cultured after each tissue was manually separated from the placenta and minced by surgical knife and scissors. Auricular cartilage-derived cells, periostium-derived cells, dermal fibroblasts, and cortical bone-derived cells started to be cultured after each tissue was manually separated from surgical specimens from patients with polydactyly or microtia. Keratocytes and scleral cells were obtained from corneal stroma and sclera (also see the Materials and Methods section). "Endometrium" was obtained from the homogenized endometrial cells under liquid nitrogen. All cells were harvested under signed informed consent, with the approval of the Ethics Committee of the National Institute for Child and Health Development, Tokyo. Signed informed consent was obtained from donors and the surgical specimens were irreversibly de-identified. All experiments handling human cells and tissues were performed in line with the Tenets of the Declaration of Helsinki. Global gene expression profiles of those cells are uploaded to GEO accession #GSE10934 at http://www.ncbi.nlm.nih.gov/geo/index.cgi.
P: passage. P0 and P1 represents primary cell culture and cell culture one passage after starting primary culture from tissues, respectively.
doi:10.1371/journal.pone.0003709.t001

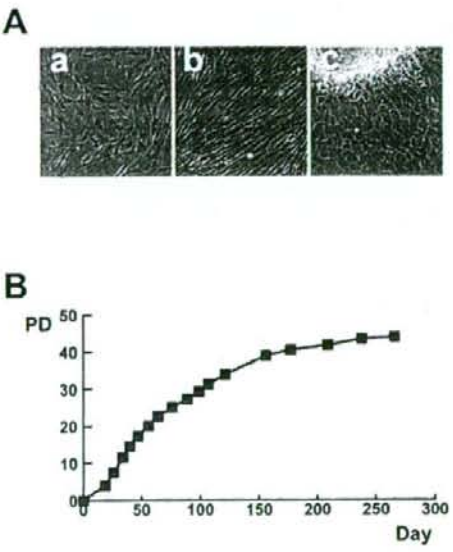

Figure 1. Proliferation of human 'sclera'-derived cells. A. Photograph of primary cultured human 'sclera'-derived cells by phase-contrast microscope. **B.** Growth curve of cultured human 'sclera'-derived cells. Vertical axis indicates population doublings (PD) and horizontal axis indicates days after innoculation of human 'sclera'-derived cells.
doi:10.1371/journal.pone.0003709.g001

Chondrogenesis of human scleral cells

After reaching 70–80% sub-confluence, we started the micromass culture of scleral cells. Four weeks after culture in a chondrogenic medium containg TGF-β1 and BMP2, a pellet of human scleral cells exhibited a spherical shape (Fig. 3A). This pellet showed an alcian blue positive extracellular matrix, indicating that cultured micromasses of scleral cells exposed to TGF-β1 and BMP2 produce an abundant matrix (Fig. 3B). RT-PCR analysis demonstrated that scleral cells at passage 0 expressed aggrecan, COL2A, SOX5, SOX6, SOX9, and PTHR1 mRNAs

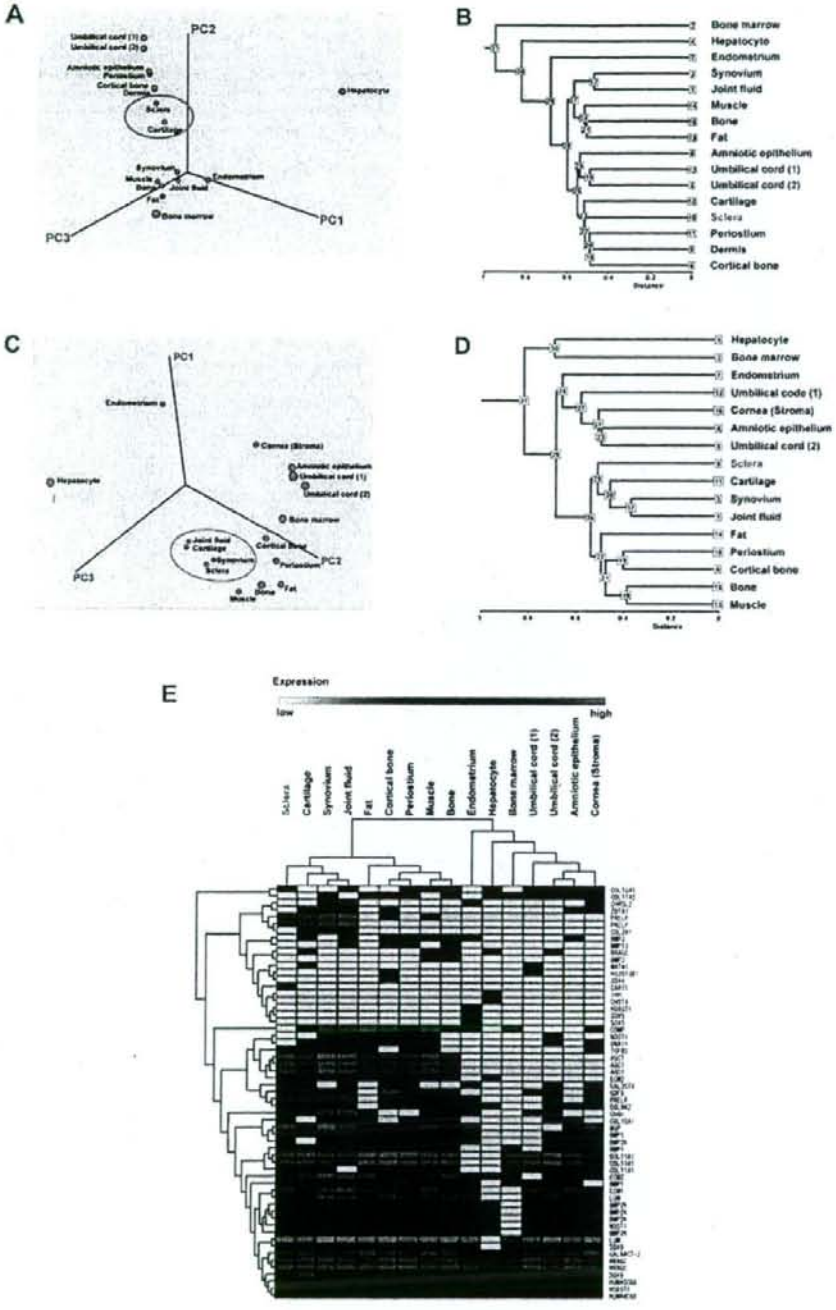

Figure 2. Global gene expression analysis of cultured human cells. A. Three-dimensional representation of PCA of gene expression levels (Human Genome U133 Plus 2.0: 54,675 probes). The gene expression data from scleral cells following one passage from the primary cultured cells (equivalent to appropriately 4 PDs) were used for PCA. Sclera and cartilage are positioned closely adjacent (shown in circle). **B.** Hierarchical clustering

analysis based on the expression of all genes (Human Genome U133 Plus 2.0: 54,675 probes, NIA Array Analysis) shows similarity between scleral cells and chondrocytes. **C**. PCA of the cartilage-associated gene expression (Table S1). Sclera, cartilage, synovium, and joint fluid are positioned closely adjacent (shown in circle). **D**. Hierarchical clustering analysis based on expression levels of the cartilage-associated genes (NIA Array Analysis). Sclera, cartilage, synovium, and joint fluid are categorized into the same group. **E**. Hierarchical clustering analysis (TIGR MeV, see the Materials & Methods) with the heat map, based on expression levels of the cartilage-associated genes. Each row represents a gene; each column represents a cell population. Sclera, cartilage, synovium, and joint fluid are categorized into the same group. Cells derived from cartilage, synovium, and joint fluid are capable of generating cartilage in vivo [7,34].
doi:10.1371/journal.pone.0003709.g002

(Fig. 3C). These expressions were maintained in the cells after 10 population doublings. After in vitro chondrogenesis of scleral cells, COL10A, SOX5, IHH, and MMP13 mRNA expressions increased. After human scleral cells labeled with DiI were implanted into a rat cartilage defect, the cells expressed type II collagen (Fig. 3D). These results demonstrated that human scleral cells retained chondrogenic potential both in vitro and in vivo.

Discussion

Tracing back of human scleral cells to chondrocytes through cultivation

This study was undertaken to investigate if human sclera has a chondrogenic nature like chicken sclera [8,9]. Bioinformatics of human scleral cells suggest similarity between scleral cells and

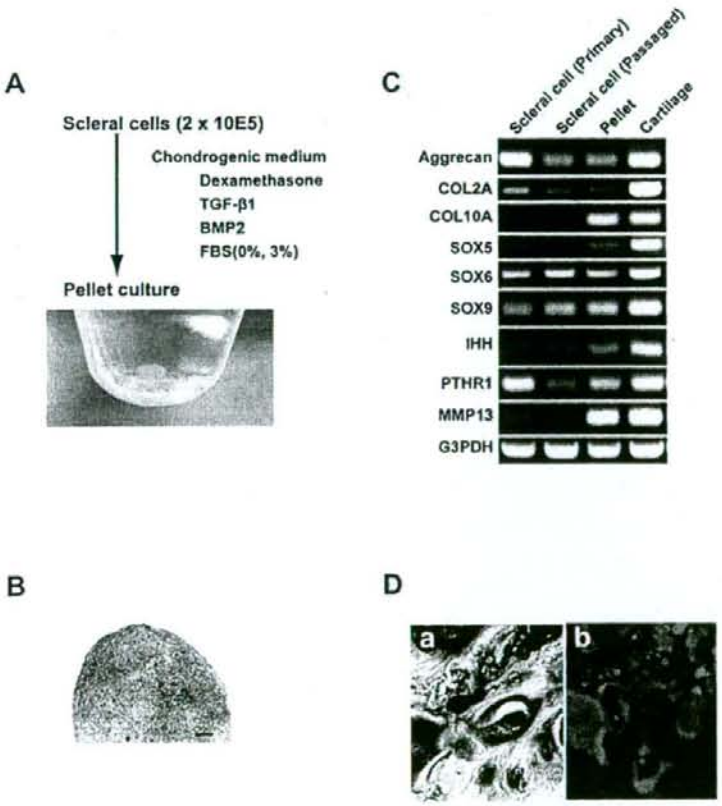

Figure 3. Chondrogenesis of human 'sclera'-derived cells. A. In vitro chondrogenesis. 'Sclera'-derived cells were centrifuged to make a pellet and cultured in chondrogenic medium for 4 weeks. Macroscopic feature is shown. **B**. Histological section of a pellet by micromass culture in a chondrogenic medium stained with alcian blue. Bar: 100 μm. **C**. Reverse transcriptase-PCR for cartilage-associated genes. Total RNAs were prepared from scleral cells at passage 0, at 10 population doublings, after in vitro chondrogenic induction, and normal cartilage as a positive control. **D**. Histological sections 4 weeks after transplantation of human scleral cells into cartilage defect of the knee in a rat. (a) Toluidin blue staining. (b) Immunohistochemistry. Human scleral cells were labeled with DiI (red). Nuclei were stained with DAPI (blue). Type II collagen was shown as green.
doi:10.1371/journal.pone.0003709.g003

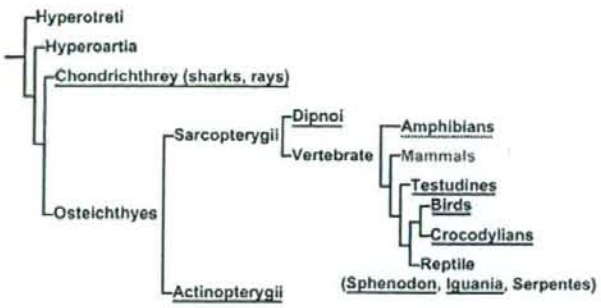

Figure 4

Figure 4. The distribution of scleral cartilage in vertebrates. The chondrogenic nature of the sclera is conserved across species. The figure is modified from Franz-Odendaal, TA, et al., 2006 [10]. Species that have cartilage in the sclera are underlined; species with either absence or presence of cartilage in the sclera, depending on family, are dot-underlined; species without cartilage in the sclera are non-underlined.
doi:10.1371/journal.pone.0003709.g004

chondrocytes, and this similarity may be attributed to evolution of the sclera (Fig. 4), that is, animals such as elasmobranch, teleost fish, amphibians, reptiles and birds incorporate the development of a cup of hyaline cartilage in the sclera [10]. Scleral cartilage is hypothesized to counter against the traction force of the extraocular muscle and against the accommodative force to move or deform the lens by intraocular muscles. In this paper, we employ the global gene expression approach to human scleral cells. As a result, scleral cells and chondrocytes are found to share common chondrogenic characteristics.

Simulation of chondrogenic process during development

The phenotype of the differentiated chondrocyte is characterized by the synthesis, deposition, and maintenance of cartilage-specific extracellular matrix molecules, including type II collagen and aggrecan [11–13]. Three-dimensional culture is a prerequisite for exhibition of this chondrogenic phenotype in vitro since the phenotype of differentiated chondrocytes is unstable in culture and is rapidly lost during serial monolayer subculturing [14–16]. The expression pattern of cartilage-associated genes in sclera-derived cells after induction is consistent with that of chondrocytes during development (Fig. 3C, Fig. S2): a) Consistent expression of type II collagen and aggrecan, markers of early-phase chondrogenesis [17,18] in sclera-derived cells, indicates that sclera-derived cells retain their chondrogenic nature as a default state; b) Induction of type X collagen and MMP13 genes after pellet formation of sclera-derived cells may simulate late-stage chondrogenesis. In addition, other chondrocyte-associated genes, such as sox5, IHH, and PTHR1 were also up-regulated. Sox5 functions as a transcription factor necessary for chondrogenesis [19,20], IHH promotes chondrogenesis as a cytokine [21], and PTHR1 mediates parathyroid hormone signaling as a specific receptor [18]. These results suggest that ex vivo culture of sclera-derived cells simulates the developmental process of chondrogenesis. Despite the chondrogenic nature of sclera-derived cells, lack of cartilage in the sclera in humans may be attributed to cis- and trans-regulation of cartilage-associated gene(s), or an unclarified inhibitory mechanism that was altered during evolution (Fig. 4).

Implication of chondrogenic nature of sclera in diseases

The fact that the gene expression pattern of the human fibrous sclera is similar to that of cartilage is interesting not only as comparative anatomy but also from a patho-etiological view point. The sclera and the joint cartilage are common targets for inflammatory cells in rheumatic arthritis [22,23] or polychondritis [24], implying common proteins between the sclera and the synovium. Although the target protein(s) remains unclarified, our findings directly explain an enigma that both the sclera and the joint cartilage are affected in rheumatic arthritis. Furthermore, mutations in genes for type II and type XI collagen are a cause of Stickler syndrome [25,26]. Patients with Stickler syndrome have joint deformity and severe high myopia due to an abnormality of the sclera. These affected lesions may be attributed to the chondrogenic nature of human sclera. In conclusion, our present study shows a chondrogenic potential of human sclera and explains the etiology of scleral disorders, at least in part. In addition, we would like to emphasize that the first database of gene expression in the human infant sclera (uploaded to GEO accession #GSE10934 at http://www.ncbi.nlm.nih.gov/geo/index.cgi) may contribute to the elucidation of scleral diseases in the future.

Materials and Methods

Isolation and cell culture of human scleral cells

Scleral tissues were excised from surgical specimens as a therapy of retinoblastoma, under signed informed consent, with the approval (approval number, #156) of the Ethics Committee of the National Institute for Child and Health Development, Tokyo. Signed informed consent was obtained from donors, and the surgical specimens were irreversibly de-identified. All experiments handling human cells and tissues were performed in line with the Tenets of the Declaration of Helsinki. The scleral pieces were cut into smaller pieces and cultured in the growth medium (GM): Dulbecco's modified Eagle's medium (DMEM)/Nutrient mixture F12 (1:1) with high glucose supplemented with 10% fetal bovine serum, insulin-transferrin-selenium, and MEM-NEAA (GIBCO).

Oligonucleotide microarray

Total RNAs were isolated from cultured scleral cells in the growth medium without any induction of differentiation to perform the gene chip analysis. Total RNA was extracted from a total of 5×10^6 cultured human scleral cells and other mesenchymal cells (Table 1) using RNeasy Plus mini-kit® (Qiagen, Maryland, USA) according to

the manufacturer's instructions. A comprehensive expression analysis was performed using 2 μg of total RNA from each sample and GeneChip® Human Genome U133 plus 2.0 probe arrays (Affymetrix, Santa Clara, CA) according to the manufacturer's instructions. To normalize the variations in staining intensity among chips, the 'Signal' values for all probes on a given chip were divided by the median value for expression of all genes on the chip. To consider genes containing only a background signal, probes were eliminated only if the 'Signal' value was less than 10, or the Detection call was 'Absent' in any sample using GeneSpring software version 7.2 (Agilent Technologies, Palo Alto). The gene chip analysis was carried out on 8 independent scleral cultures.

Hierarchical clustering and principal component analysis (PCA)

To analyze the gene expression data in an unsupervised manner by gene chip array, we used hierarchical clustering and principal component analysis (NIA Array; http://lgsun.grc.nia.nih.gov/ANOVA/ [27], TIGR MeV; http://www.tm4.org/mer.html [28]). The hierarchical clustering techniques classify data by similarity and the results are represented by dendrogram. PCA is a multivariate analysis technique which finds major patterns in data variability. Hierarchical clustering and PCA were performed on the data of gene chip analysis (a single assay for each sample) to group scleral cells and other mesenchymal cells into subcategories (Table 1).

In vitro chondrogenesis

Two hundred thousand scleral cells were placed in a 15-ml polypropylene tube (Becton Dickinson) and centrifuged for 10 minutes. The pellet was cultured in DF-C medium™ containing 0.1 μM dexamethasone, 1 mM sodium pyruvate, 0.17 mM ascorbic acid-2-phosphate, 0.35 mM proline, 6.25 μg/ml bovine insulin, 6.25 μg/ml transferrin, 6.25 μg/ml selenous acid, 5.33 μg/ml linoleic acid, 1.25 mg/ml BSA, 5 ng/ml TGF-β1, 5 ng/ml BMP2, and 3% fetal bovine serum (TOYOBO). The medium was replaced every 3 to 4 days for 28 days. For microscopy, the pellets were embedded in paraffin, cut into 5-μm sections, and stained with alcian blue [29,30].

In vivo chondrogenesis

Under anesthesia, full thickness cartilage defects were created in the trochlear groove of the femur in SD rats. The defects were filled with DiI-labeled human scleral cells. The rats were returned to their cages after the operation and allowed to move freely. Animals were sacrificed with an overdose of sodium pentobarbital at 4 weeks after the operation. Specimens were dissected and embedded in paraffin. The sections were stained with toluidine blue and immunohistochemically stained with anti-type II collagen antibodies (clone F-57, DAIICHI FINE CHEMICAL, Co. Ltd., Toyama, Japan). All animals received humane care in compliance with the "Principles of Laboratory Animal Care" formulated by the National Society for Medical Research and the "Guide for the Care and Use of Laboratory Animals" prepared by the Institute of Laboratory Animal Resources and published by the US National Institutes of Health (NIH Publication No. 86-23, revised 1985). The operation protocols were accepted by the Laboratory Animal Care and Use Committee of the Research Institute for Child and Health Development (2003-002).

Reverse transcriptase-PCR

Total RNA was isolated with an RNeasy Plus mini-kit. Cartilage pellets were digested with 3 mg/ml Collagenase D for 3 hours at 37°C.

The following PCR primer sets were used for cartilage-associated genes: aggrecan, sense (5′-TACACTGGCGAGCACTGTAAC -3′) and antisense (5′-CAGTGGCCCTGGTACTTGTT-3′), product size, 71 bp; collagen, type II, alpha 1, sense (5′-TTCAGCTATG-GAGATGACAATC -3′) and antisense (5′-AGAGTCCTAGAGT-GACTGAG -3′), product size, 472 bp; collagen, typeX, alpha 1, sense (5′-CACCTTCTGCACTGCTCATC-3′) and antisense (5′-GGCAGCATATTCTCAGATGGA-3′), product sizem, 104 bp; SOX5, sense (5′-AGCCAGAGTTAGCACAATAGG -3′) and antisense (5′-CATGATTGCCTTGTATTC -3′), product size, 619 bp; SOX6, sense (5′-ACTGTGGCTGAAGCACGAGTC -3′) and antisense (5′-TCCGCCATCTGTCTTCATACC -3′), product size, 562 bp; SOX9, sense (5′-GTACCCGCACTTGCACAAC-3′) and antisense (5′-TCGCTCTCGTTCAGAAGTCTC-3′), product size 72 bp; Indian hedgehog homolog (IHH), sense (5′-TGCATTGCT-CCGTCAAGTC-3′) and antisense (5′-CCACTCTCCAGGCG-TACCT-3′), product size 88 bp; parathyroid hormone receptor 1(PTHR1), sense (5′-CCTGAGTCTGAGGAGGACAAG-3′) and antisense (5′-CACAGGATGTGGTCCCATT-3′), product size 86 bp; matrix metallopeptidase 13 (MMP13), sense (5′-CCAGTCTCC-GAGGAGAAACA-3′) and antisense (5′-AAAAACAGCTCCG-CATCAAC-3′),product size, 85 bp, and GAPDH, sense (5′-GCTCAGACACCATGGGGAAGGT-3′) and antisense (5′-GTGGTGCAGGAGGCATTGCTGA-3′), product size, 474 bp.

Supporting Information

Figure S1 Global gene expression analysis of cultured human cells. Hierarchical clustering analysis based on expression levels of the cartilage-associated genes (NIA Array Analysis). We performed gene chip analysis (a single assay for each analysis) for eight independent primary scleral cultures from five patients (donors). We started eight independent cultures from three different scleral sites of Donor 2 (e.g. the anterior site 1.5 mm apart from the limbs, the middle part, and the posterior part), 2 different scleral sites of Donor 5, and three scleral sites of Donor 1, 3, and 4. We performed hierarchical clustering analysis, using these independent cultures and obtained consistent results, that is, "sclera"-derived cells are categorized into one sub-group. Furthermore, the sclera, cartilage, synovium, and joint fluid are categorized into the same group.
Found at: doi:10.1371/journal.pone.0003709.s001 (0.07 MB PDF)

Figure S2 Cartilage-associated gene expressions in cultured fibroblasts derived from the dermis and the sclera. Cartilage-associated gene expressions by RT-PCR in cultured fibroblasts derived from the dermis and the sclera. Aggrecan, COL2A, IHH and PTHR mRNA expressions were clearly stronger in the scleral fibroblasts compared to the dermal fibroblasts, indicating that chondrogenic nature could be specific for the sclera among collagenous tissues.
Found at: doi:10.1371/journal.pone.0003709.s002 (0.01 MB PDF)

Table S1 Cartilage-associated genes
Found at: doi:10.1371/journal.pone.0003709.s003 (0.01 MB PDF)

Acknowledgments

We would like to express our sincere thanks to T. Tang for helping with animal experiments and T. Sugiki, M. Nasu, A. Kawakita and M. Toyoda for their discussion of this work.

Author Contributions

Conceived and designed the experiments: YS NA TM IS AU. Performed the experiments: YS NA HM TM IS. Analyzed the data: YS YT KM HS IS. Contributed reagents/materials/analysis tools: YS NA IS. Wrote the paper: YS KM HS IS AU.

References

1. Connon CJ, Meek KM, Kinoshita S, Quantock AJ (2004) Spatial and temporal alterations in the collagen fibrillar array during the onset of transparency in the avian cornea. Exp Eye Res 78: 909–915.
2. Yoshida S, Shimmura S, Shimazaki J, Shinozaki N, Tsubota K (2005) Serum-free spheroid culture of mouse corneal keratocytes. Invest Ophthalmol Vis Sci 46: 1653–1658.
3. Zhou J, Rappaport EF, Tobias JW, Young TL (2006) Differential gene expression in mouse sclera during ocular development. Invest Ophthalmol Vis Sci 47: 1794–1802.
4. Young TL, Guo XD, King RA, Johnson JM, Rada JA (2003) Identification of genes expressed in a human scleral cDNA library. Mol Vis 9: 508–514.
5. Sakaguchi Y, Sekiya I, Yagishita K, Muneta T (2005) Comparison of human stem cells derived from various mesenchymal tissues: superiority of synovium as a cell source. Arthritis Rheum 52: 2521–2529.
6. Yoshimura H, Muneta T, Nimura A, Yokoyama A, Koga H, et al. (2007) Comparison of rat mesenchymal stem cells derived from bone marrow, synovium, periosteum, adipose tissue, and muscle. Cell Tissue Res 327: 449–462.
7. Koga H, Muneta T, Ju YJ, Nagase T, Nimura A, et al. (2007) Synovial stem cells are regionally specified according to local microenvironments after implantation for cartilage regeneration. Stem Cells 25: 689–696.
8. Seko Y, Shimokawa H, Tokoro T (1995) Expression of bFGF and TGF-beta 2 in experimental myopia in chicks. Invest Ophthalmol Vis Sci 36: 1183–1187.
9. Seko Y, Tanaka Y, Tokoro T (1995) Influence of bFGF as a potent growth stimulator and TGF-beta as a growth regulator on scleral chondrocytes and scleral fibroblasts in vitro. Ophthalmic Res 27: 144–152.
10. Franz-Odendaal TA, Hall BK (2006) Skeletal elements within teleost eyes and a discussion of their homology. J Morphol 267: 1326–1337.
11. Archer CW, McDowell J, Bayliss MT, Stephens MD, Bentley G (1990) Phenotypic modulation in sub-populations of human articular chondrocytes in vitro. J Cell Sci 97 (Pt 2): 361–371.
12. Hauselmann HJ, Fernandes RJ, Mok SS, Schmid TM, Block JA, et al. (1994) Phenotypic stability of bovine articular chondrocytes after long-term culture in alginate beads. J Cell Sci 107 (Pt 1): 17–27.
13. Reginato AM, Iozzo RV, Jimenez SA (1994) Formation of nodular structures resembling mature articular cartilage in long-term primary cultures of human fetal epiphyseal chondrocytes on a hydrogel substrate. Arthritis Rheum 37: 1338–1349.
14. Benya PD, Shaffer JD (1982) Dedifferentiated chondrocytes reexpress the differentiated collagen phenotype when cultured in agarose gels. Cell 30: 215–224.
15. Bonaventure J, Kadhom N, Cohen-Solal L, Ng KH, Bourguignon J, et al. (1994) Reexpression of cartilage-specific genes by dedifferentiated human articular chondrocytes cultured in alginate beads. Exp Cell Res 212: 97–104.
16. Lefebvre V, Peeters-Joris C, Vaes G (1990) Production of collagens, collagenase and collagenase inhibitor during the dedifferentiation of articular chondrocytes by serial subcultures. Biochim Biophys Acta 1051: 266–275.
17. Pittenger MF, Mackay AM, Beck SC, Jaiswal RK, Douglas R, et al. (1999) Multilineage potential of adult human mesenchymal stem cells. Science 284: 143–147.
18. Shukunami C, Shigeno C, Atsumi T, Ishizeki K, Suzuki F, et al. (1996) Chondrogenic differentiation of clonal mouse embryonic cell line ATDC5 in vitro: differentiation-dependent gene expression of parathyroid hormone (PTH)/PTH-related peptide receptor. J Cell Biol 133: 457–468.
19. Lefebvre V, Li P, de Crombrugghe B (1998) A new long form of Sox5 (L-Sox5), Sox6 and Sox9 are coexpressed in chondrogenesis and cooperatively activate the type II collagen gene. Embo J 17: 5718–5733.
20. Sekiya I, Tsuji K, Koopman P, Watanabe H, Yamada Y, et al. (2000) SOX9 enhances aggrecan gene promoter/enhancer activity and is up-regulated by retinoic acid in a cartilage-derived cell line, TC6. J Biol Chem 275: 10738–10744.
21. Kobayashi T, Soegiarto DW, Yang Y, Lanske B, Schipani E, et al. (2005) Indian hedgehog stimulates periarticular chondrocyte differentiation to regulate growth plate length independently of PTHrP. J Clin Invest 115: 1734–1742.
22. Jayson MI, Jones DE (1971) Scleritis and rheumatoid arthritis. Ann Rheum Dis 30: 343–347.
23. Barr CC, Davis H, Culbertson WW (1981) Rheumatoid scleritis. Ophthalmology 88: 1269–1273.
24. Isaak BL, Liesegang TJ, Michet CJ Jr (1986) Ocular and systemic findings in relapsing polychondritis. Ophthalmology 93: 681–689.
25. Annunen S, Korkko J, Czarny M, Warman ML, Brunner HG, et al. (1999) Splicing mutations of 54-bp exons in the COL11A1 gene cause Marshall syndrome, but other mutations cause overlapping Marshall/Stickler phenotypes. Am J Hum Genet 65: 974–983.
26. Van Camp G, Snoeckx RL, Hilgert N, van den Ende J, Fukuoka H, et al. (2006) A new autosomal recessive form of Stickler syndrome is caused by a mutation in the COL9A1 gene. Am J Hum Genet 79: 449–457.
27. Sharov AA, Dudekula DB, Ko MS (2005) A web-based tool for principal component and significance analysis of microarray data. Bioinformatics 21: 2548–2549.
28. Saeed AI, Sharov V, White J, Li J, Liang W, et al. (2003) TM4: a free, open-source system for microarray data management and analysis. Biotechniques 34: 374–378.
29. Sugiki T, Uyama T, Toyoda M, Morioka H, Kume S, et al. (2007) Hyaline cartilage formation and enchondral ossification modeled with KUM5 and OP9 chondroblasts. J Cell Biochem 100: 1240–1254.
30. Sekiya I, Larson BL, Vuoristo JT, Reger RL, Prockop DJ (2005) Comparison of effect of BMP-2, -4, and -6 on in vitro cartilage formation of human adult stem cells from bone marrow stroma. Cell Tissue Res 320: 269–276.
31. Morito T, Muneta T, Hara K, Ju YJ, Mochizuki T, et al. (2008) Synovial fluid-derived mesenchymal stem cells increase after intra-articular ligament injury in humans. Rheumatology (Oxford) 47: 1137–1143.
32. Segawa Y, Muneta T, Makino M, Nimura A, Mochizuki T, et al. (in press) Mesenchymal stem cells derived from synovium, meniscus, anterior cruciate ligament, and articular chondrocytes share similar gene expression profiles. Journal of Orthopaedic Research.
33. Tsuruga Y, Kiyono T, Matsushita M, Takahashi T, Kasai N, et al. (2008) Effect of intrasplenic transplantation of immortalized human hepatocytes in the treatment of acetaminophen-induced acute liver failure SCID mice. Transplant Proc 40: 617–619.
34. Mochizuki T, Muneta T, Sakaguchi Y, Nimura A, Yokoyama A, et al. (2006) Higher chondrogenic potential of fibrous synovium- and adipose synovium-derived cells compared with subcutaneous fat-derived cells: distinguishing properties of mesenchymal stem cells in humans. Arthritis Rheum 54: 843–853.

The fusing ability of sperm is bestowed by CD9-containing vesicles released from eggs in mice

Kenji Miyado*[†‡§], Keiichi Yoshida[‡¶], Kazuo Yamagata[‖], Keiichi Sakakibara*, Masaru Okabe**, Xiaobiao Wang*, Kiyoko Miyamoto*, Hidenori Akutsu*, Takahiko Kondo*, Yuji Takahashi*, Tadanobu Ban[††], Chizuru Ito[¶], Kiyotaka Toshimori[¶], Akihiro Nakamura*, Masahiko Ito*, Mami Miyado*, Eisuke Mekada**, and Akihiro Umezawa*

*National Center for Child Health and Development, 2-10-1 Okura, Setagaya, Tokyo 157-8535, Japan; [†]School of Biomedical Science, Tokyo Medical and Dental University, Yushima, Bunkyo, Tokyo 113-8510, Japan; [¶]Graduate School of Medicine, Chiba University, 1-8-1 Inohana, Chuo-ku, Chiba 260-8670, Japan; [‖]Center for Developmental Biology, RIKEN Kobe Institute, 2-2-3 Minatojima-minamimachi, Chuo-ku, Kobe, Hyogo 650-0047, Japan; and **Research Institute for Microbial Diseases, and [††]Faculty of Medicine, Osaka University, 3-1 Yamadaoka, Suita, Osaka 565-0871, Japan

Edited by Ryuzo Yanagimachi, University of Hawaii, Honolulu, HI, and approved July 8, 2008 (received for review November 8, 2007)

Membrane fusion is an essential step in the encounter of two nuclei from sex cells—sperm and egg—in fertilization. However, aside from the involvement of two molecules, CD9 and Izumo, the mechanism of fusion remains unclear. Here, we show that sperm–egg fusion is mediated by vesicles containing CD9 that are released from the egg and interact with sperm. We demonstrate that the CD9$^{-/-}$ eggs, which have a defective sperm-fusing ability, have impaired release of CD9-containing vesicles. We investigate the fusion-facilitating activity of CD9-containing vesicles by examining the fusion of sperm to CD9$^{-/-}$ eggs with the aid of exogenous CD9-containing vesicles. Moreover, we show, by examining the fusion of sperm to CD9$^{-/-}$ eggs, that hamster eggs have a similar fusing ability as mouse eggs. The CD9-containing vesicle release from unfertilized eggs provides insight into the mechanism required for fusion with sperm.

fertilization | membrane fusion | EGFP | exosome

Fertilization is an essential process that naturally produces a cell capable of developing into a new individual. It consists of sequential events, including membrane fusion of sperm and egg (1). Despite the importance of understanding fertilization in controlling human reproduction and preserving endangered species, the molecular basis underlying the fusion remains a mystery, however. Previously, we reported that a tetraspan-membrane protein (tetraspanin), CD9, is expressed on the egg plasma membrane and is required for sperm–egg fusion (2–4). A role of CD9 in other fusion events also has been demonstrated (5). When sperm are added to eggs from CD9$^{-/-}$ females, the sperm bind to the egg plasma membrane normally, but fusion is severely impaired (2–4). Two recent observations suggest that CD9 plays a role in the organization of egg membrane. First, CD9 is transferred from the egg to the fertilizing sperm present in the perivitelline space (PVS) (6), suggesting the involvement of a process similar to trogocytosis, a mechanism of cell-to-cell contact-dependent transfer of membrane fragments (7). Second, CD9 deficiency alters the length and density of microvilli on the egg plasma membrane (8). CD9 is also known to be a component of exosomes, membrane vesicles released from a wide range of cells (9, 10). Despite its relationship to CD9, the involvement of exosome release in sperm–egg fusion remains unknown. In the present study, we analyzed the potential of enhanced green fluorescent protein (EGFP)-tagged CD9 (CD9-EGFP) as a reporter protein to study sperm–egg fusion in living mouse eggs.

Results

To observe the movement of CD9 during sperm–egg fusion, we generated a transgenic mouse line that expressed CD9-EGFP only in eggs (Fig. 1*A*), and converted to the genetic background of CD9$^{-/-}$ mice by mating mice. Western blot analysis using anti-CD9 monoclonal antibody (mAb) revealed that an expected CD9-EGFP with a molecular mass of 51 kDa (CD9 and EGFP contributing to 24 and 27 kDa, respectively) was expressed in the eggs collected from Tg^{+}CD9$^{-/-}$ mice; however, the amount of CD9-EGFP expressed in CD9$^{-/-}$ eggs was estimated to be 10% of that of endogenous CD9 in the CD9$^{+/+}$ eggs (Fig. 1*B*). Despite the small amount of CD9-EGFP expressed in eggs, CD9-EGFP demonstrated the ability to reverse the sterility of CD9$^{-/-}$ females (Fig. 1*C*). The numbers of pups obtained from Tg^{+}CD9$^{-/-}$ females (6.4 ± 0.5) were similar to those from

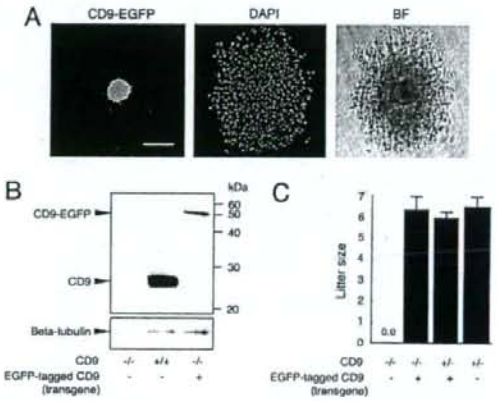

Fig. 1. Generation of mice expressing CD9-EGFP in eggs. (*A*) CD9-EGFP specifically expressed in eggs with mouse ZP3-promoter. Cumulus oocyte complex from Tg^{+}CD9$^{+/+}$ oviducts was collected at 14 h after injection of human chorionic gonadotropin. Nuclei of an egg and cumulus cells were counterstained with DAPI. (*Left*) CD9-EGFP. (*Center*) DAPI. (*Right*) Bright field. Scale bar: 100 μm. (*B*) Western blot analysis for eggs collected from CD9$^{-/-}$, CD9$^{+/+}$, and Tg^{+}CD9$^{-/-}$ mice. The same amounts, including 30 eggs of each lysate, were examined by anti-CD9 and anti-beta-tubulin mAbs (internal control). (*C*) Litter sizes of CD9$^{-/-}$ (n = 31), Tg^{+}CD9$^{-/-}$ (n = 35), Tg^{+}CD9$^{+/-}$ (n = 16), and CD9$^{+/-}$ mice (n = 15) (mean ± SEM). The numbers of females examined are in parentheses.

Author contributions: K. Miyado, K. Yamagata, M.O., and A.U. designed research; K. Miyado, K. Yoshida, K.S., X.W., K. Miyamoto, H.A., T.K., Y.T., T.B., C.I., A.N., M.I., and M.M. performed research; K. Miyado contributed new reagents/analytic tools; K. Miyado, K. Yoshida, H.A., K.T., E.M., and A.U. analyzed data; and K. Miyado wrote the paper.

The authors declare no conflicts of interest.

This article is a PNAS Direct Submission.

Freely available online through the PNAS open access option.

[‡]K. Miyado and K. Yoshida contributed equally to this work.

[§]To whom correspondence should be addressed. E-mail: kmiyado@nch.go.jp.

This article contains supporting information online at www.pnas.org/cgi/content/full/0710608105/DCSupplemental.

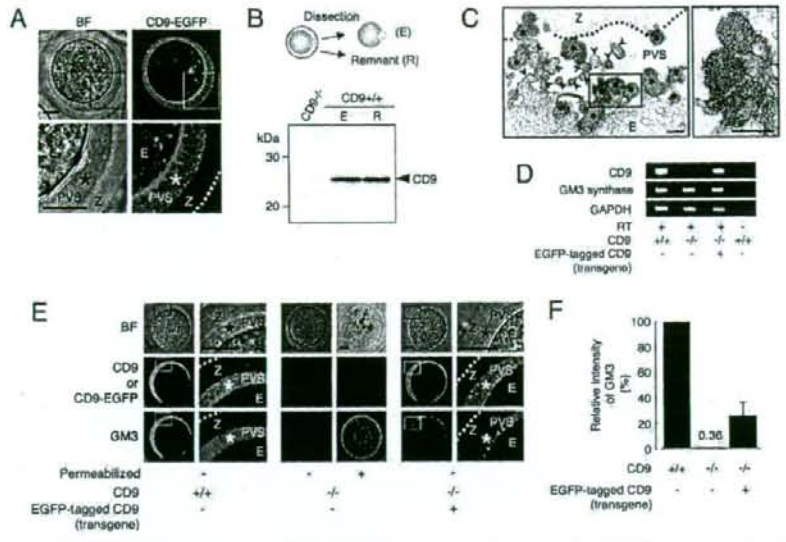

Fig. 2. Identification of secretory vesicles containing CD9 from unfertilized eggs. *A*, A single confocal image showing CD9-EGFP in unfertilized $Tg^+CD9^{-/-}$ eggs (E), including the PVS (*), zona pellucida (Z), and the outer margin of the zona pellucida (dotted line). (*Left*) Bright field. (*Right*) CD9-EGFP. *Lower* are enlarged images of the boxed areas. (*B*) Western blot analysis for eggs mechanically fractionated as shown in the diagram: zona-intact $CD9^{-/-}$ eggs (E) (10 eggs per lane) and zona-free $CD9^{+/+}$ eggs (10 eggs per lane). The medium (R) containing the remnant material from 40 eggs treated with a piezo manipulator was loaded in each lane. (*C*) Immunoelectron-microscopic analysis of $CD9^{+/+}$ eggs. The zona-intact $CD9^{+/+}$ eggs were examined using anti-CD9-mAb and 5-nm gold beads conjugated with anti-rat IgG Ab. Left panel: Image including CD9-containing vesicles (*), microvilli (arrowheads), zona pellucida (Z), perivitelline space (PVS), and egg (E). (*Right*) An enlarged image of the boxed region in the left panel. Scale bar: 200 nm. (*D*) RT-PCR for CD9, GM3 synthase, and glyceraldehyde-3-phosphate dehydrogenase transcripts in $CD9^{+/+}$, $CD9^{-/-}$, and $Tg^+CD9^{-/-}$ eggs. The same amounts, including 50 eggs in each reaction, were examined. The right end lanes are negative controls in which RT was removed from reactions of wild-type eggs. (*E*) Localization of GM3 and CD9 in $CD9^{+/+}$, $CD9^{-/-}$, and $Tg^+CD9^{-/-}$ eggs. (*Left*) Wild-type. (*Middle*) $CD9^{-/-}$. (*Right*) $Tg^+CD9^{-/-}$. Right-side of the sets of wild-type and $Tg^+CD9^{-/-}$ eggs are enlarged images of the boxed regions. The live eggs were examined, and the internal localization of GM3 in $CD9^{-/-}$ eggs was examined under fixed, permeabilized conditions. (*F*) Comparison of the fluorescent intensities of GM3 stained by antibody in wild-type (n = 10), $CD9^{-/-}$ (n = 9), and $Tg^+CD9^{-/-}$ eggs (n = 10) (mean ± SEM). The average values of the wild-type eggs were set to 100%.

$Tg^+CD9^{+/-}$ and $CD9^{+/-}$ females (6.0 ± 0.2 and 6.5 ± 0.5) and greater than those from $CD9^{-/-}$ females (0.0 ± 0.0). The $CD9^{+/-}$ females did not exhibit any loss in fertility that could cause a reduction of litter size relative to that of the $CD9^{+/+}$ females (4). Furthermore, the transgene had no effect on normal fertility. These results demonstrate that transgenically expressed CD9-EGFP can compensate for the loss of intrinsic CD9 and yield eggs with the ability to fuse with sperm.

Based on the foregoing evidence, we observed the subcellular localization of CD9-EGFP in "living" $Tg^+CD9^{-/-}$ eggs (Fig. 2*A*). As expected, confocal microscopic analysis allowed the visualization of two types of CD9-EGFP localization: intense on the plasma membrane and also in the cytoplasm. Unexpectedly, we found loosely filled, noncompacted CD9-EGFP in the PVS, a space formed between the zona pellucida and the plasma membrane of the egg. The localization of CD9 outside the eggs also was confirmed by Western blot analysis using anti-CD9 mAb (Fig. 2*B*). As shown in the diagram, $CD9^{+/+}$ eggs were mechanically fractionated into denuded eggs and other components (R) using a piezo manipulator (11). The fraction R, containing the zona pellucida and the components in the PVS, was centrifuged and subjected to Western blot analysis. The amount of CD9 in the remnant material from 40 eggs was found to be densitometrically equal to that of 10 zona-free eggs, demonstrating an estimated relative abundance of CD9 in the remnant of 20% per egg. Subsequently, we performed immunoelectron-microscopic analysis on the $CD9^{+/+}$ eggs. We identified the vesicles bound to gold particles inside the PVS (Fig. 2*C*). The sectioned microvilli contained a branched network of actin filaments, whereas the variously sized vesicles (50–250 nm in diameter) had uniformly dense materials rather than actin filaments. We also compared $CD9^{+/+}$, $Tg^+CD9^{-/-}$, and $CD9^{-/-}$ eggs by electron-microscopic analysis [supporting information (SI) Fig. S1]. The accumulation of vesicles in the PVS in the $Tg^+CD9^{-/-}$ eggs was comparable to that in the $CD9^{+/+}$ eggs, whereas it was not seen in the $CD9^{-/-}$ or germinal vesicle-staged $CD9^{+/+}$ eggs. These results indicate that 20% of the total amount of CD9 is stored as vesicles in the PVS during meiosis.

We next examined the expression of ganglioside GM3, identified as a CD9-associated molecule (12) and a component of exosomes (10), in $CD9^{+/+}$, $CD9^{-/-}$, and $Tg^+CD9^{-/-}$ eggs. First, we confirmed the expression of GM3 synthase (ST3GalV/SAT-1) (13) in these eggs by RT-PCR (Fig. 2*D*). Then we investigated the localization of GM3 by immunostaining these live eggs with anti-GM3 mAb (Fig. 2*E*). This antibody has been demonstrated to recognize GM3 in the plasma membrane of cells without treatment for permeabilization (14). Finally, we measured the fluorescent intensities of GM3 in these live eggs (Fig. 2*F*). As expected, in wild-type eggs, GM3 was colocalized with CD9 in the PVS and plasma membrane (Fig. 2*E Left* and Fig. 2*F*). In contrast, in $CD9^{-/-}$ eggs, the fluorescent intensities of GM3 were decreased dramatically in the PVS and plasma membrane (0.4% ± 0.2%, relative to 100% for the $CD9^{+/+}$ eggs), consistent with the loss of CD9 (Fig. 2*E Center* and Fig. 2*F*), whereas GM3 could be detected in the cytoplasm of $CD9^{-/-}$ eggs that had been permeabilized by a detergent after fixation. Moreover, the expression of CD9-EGFP reversed the decrease of GM3 in the PVS and plasma membrane of $CD9^{-/-}$ eggs (25.6 ± 10.7%) (Fig. 2*E Right* and Fig. 2*F*), corresponding to the amount of CD9-EGFP quantified by Western blot analysis (Fig. 1*B*). In addition, electron-microscopic analysis revealed that the number of characteristic membrane structures, termed microvilli (1), were significantly decreased in the $CD9^{-/-}$ eggs compared with the $CD9^{+/+}$ eggs (Fig. S2 *A* and *B*). The numbers of microvilli were increased by ≈50% by the expression of CD9-EGFP in the $CD9^{-/-}$ eggs. The analyses of three types of eggs indicate that CD9- and GM3-containing vesicle release is linked to microvilli formation.

We next investigated the involvement of CD9-containing vesicles in sperm–egg fusion (Fig. 3). We found that, based on the length of microvilli (Fig. S2*C*), zona-intact $Tg^+CD9^{-/-}$ eggs can be categorized into two groups (Fig. 3*A*). From single

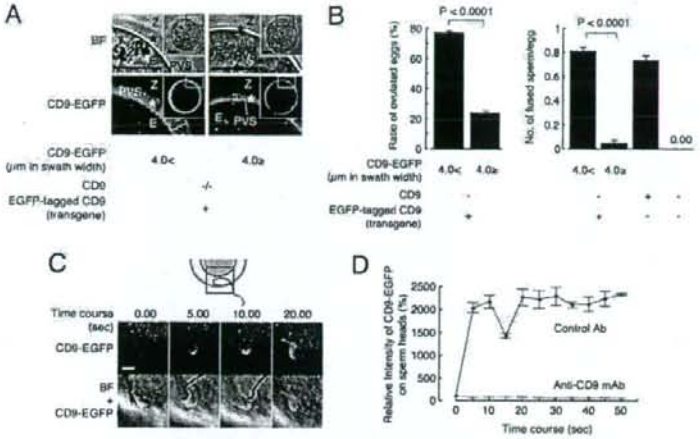

Fig. 3. Involvement of CD9-containing vesicles in sperm–egg fusion. (*A*) Categorization of $Tg^+CD9^{-/-}$ eggs (E) into two groups according to the thickness of CD9-EGFP in the PVS (*) and the inner region of the zona pellucida (Z) (>4.0 μm or ≤ 4.0 μm), indicated by double-headed lines. The boxed regions in *Insets* are enlarged. Scale bar: 20 μm. (*B*) Comparison of the fusing ability of two groups of $Tg^+CD9^{-/-}$ eggs with wild-type sperm. Left graph: Ratio of two groups of $Tg^+CD9^{-/-}$ eggs ovulated from 12 females (mean ± SEM). Right graph: Number of sperm fused per egg in two groups of zona-intact $Tg^+CD9^{-/-}$ eggs ovulated from 12 females (>4.0 μm, $n = 204$; ≤4.0 μm, $n = 66$) (mean ± SEM). $CD9^{+/+}$ ($n = 120$) and $CD9^{-/-}$ ($n = 112$) served as positive and negative controls, respectively. (*C* and *D*) Monitoring of the association of egg CD9-containing vesicles with wild-type sperm. $Tg^+CD9^{-/-}$ eggs were incubated with the sperm and monitored immediately after the sperm penetrated the zona pellucida under the presence of anti-CD9 mAb (boxed region). The values were calculated from data scanning by confocal microscopy (15 sperm in triplicate dishes) Blue: Preimmune rat IgG. Red: Anti-CD9 mAb (KMC8) (mean ± SEM). The average values of the fluorescent intensities of CD9-EGFP at 0 s were set to 100%, and the final concentration of antibodies was adjusted to 50 μg/ml. Scale bar, 5 μm.

confocal images sectioned through the largest diameter, the accumulation of CD9-EGFP from the plasma membrane to the inner region of the zona pellucida was >4.0 μm in swath width in one group and ≤ 4.0 μm in the other group. The accumulation of CD9-EGFP was predicted to show that CD9-containing vesicles are more highly accumulated within the PVS in the >4.0-μm group compared with the ≤ 4.0-μm group. Comparing the ratio of these two groups in $Tg^+CD9^{-/-}$-ovulated eggs revealed a much higher percentage of the >4.0-μm group (77.0 ± 1.3% vs.23.7 ± 1.5%) (Fig. 3*B Left*). Therefore, we focused on the heterogeneity of CD9-EGFP accumulation within the PVS and determined the ratio of the two groups in zona-intact $Tg^+CD9^{-/-}$ eggs that successfully fused with the sperm 6 h after insemination. The >4.0-μm group of $Tg^+CD9^{-/-}$ eggs showed higher activity for fusion with sperm (0.81 ± 0.04 sperm fused per egg), compared with the ≤40-μm group of $Tg^+CD9^{-/-}$ eggs (0.05 ± 0.03) and the $CD9^{-/-}$ eggs (0.00 ± 0.00), and comparable activity to that of wild-type eggs (0.73 ± 0.04) (Fig. 3*B Right*). The average activity of all $Tg^+CD9^{-/-}$ eggs (0.72 ± 0.03 sperm fused per egg) was equal to that of wild-type eggs (0.73 ± 0.04 sperm fused per egg). The difference between the two groups of $Tg^+CD9^{-/-}$ eggs was statistically significant (Fig. 3*B*). These results suggest that the quantities of CD9-containing vesicles, as assessed by the swath width of CD9-EGFP, are strongly correlated with the frequency of sperm–egg fusion.

To detect the association between sperm and CD9-containing vesicles, we serially monitored the wild-type sperm that penetrated the zona pellucida of the $Tg^+CD9^{-/-}$ eggs (Fig. 3 *C* and *D*). As shown in the diagram, we began monitoring the sperm immediately after the head portion of sperm penetrated the zona pellucida of the $Tg^+CD9^{-/-}$ eggs (Fig. 3*C Upper*, boxed area in the diagram). Soon after we began to monitor the sperm, the fluorescent intensities of CD9-EGFP on the sperm heads increased and then decreased rapidly between 0 s and 15 s, then increased again, reaching a maximum at 20 s. At this point, the CD9-EGFP fully covered the surface of the sperm heads. In contrast, when the sperm were incubated with $Tg^+CD9^{-/-}$ eggs in the medium containing anti-CD9 mAb, no increase in intensity of CD9-EGFP on the sperm heads was detected. Anti-CD9 mAbs have been reported to inhibit sperm–egg fusion (4, 15, 16). Our findings demonstrate that the anti-CD9 mAb inhibited the association of sperm with CD9-containing vesicles in parallel to inhibition of sperm–egg fusion.

To determine whether CD9-containing vesicles are capable of initiating sperm–egg fusion, we incubated the sperm with $CD9^{-/-}$ eggs in medium containing the vesicles collected from $CD9^{+/+}$ eggs (Fig. 4 and Fig. S3). To restrict the source of CD9 into the vesicles from the $CD9^{+/+}$ eggs, we used sperm collected from the epididymis of $CD9^{-/-}$ males. We estimated the capability of the vesicles to influence fusion by counting the number of sperm fused with $CD9^{-/-}$ eggs. As shown in the experimental design, after the zona pellucida was removed from the $CD9^{-/-}$ eggs, the eggs were incubated with sperm in the medium containing the vesicles (Fig. 4*A*). When examined at 1 h after incubation, the sperm were seen to be capable of fusing with $CD9^{-/-}$ eggs after co-incubation with the vesicles (Fig. 4*A Center*), indicating restoration of the fusibility of $CD9^{-/-}$ eggs with the sperm (0.58 ± 0.07 sperm fused per egg) (Fig. 4*B*). We detected further evidence of sperm–egg fusion in the $CD9^{-/-}$ eggs from which a second polar body had been extruded. In contrast, we did not detect improved fusibility of sperm with eggs in medium depleted of CD9-containing vesicles using beads conjugated with anti-CD9 mAb (Fig. 4*A Right* and *B*). After treatment with the beads, the quantity of CD9 in the depleted medium was significantly decreased, to 16% of the untreated medium (Fig. 4*C*). In addition, $CD9^{-/-}$ remnants failed to rescue the fusing ability of $CD9^{-/-}$ eggs. These findings indicate that the association with CD9-containing vesicles renders the sperm capable of fusing with eggs without endogenous CD9 expression. We estimated the relative abundance of CD9 in the remnant as 18% of the total amount in the eggs (Fig. 4*C*). We further found

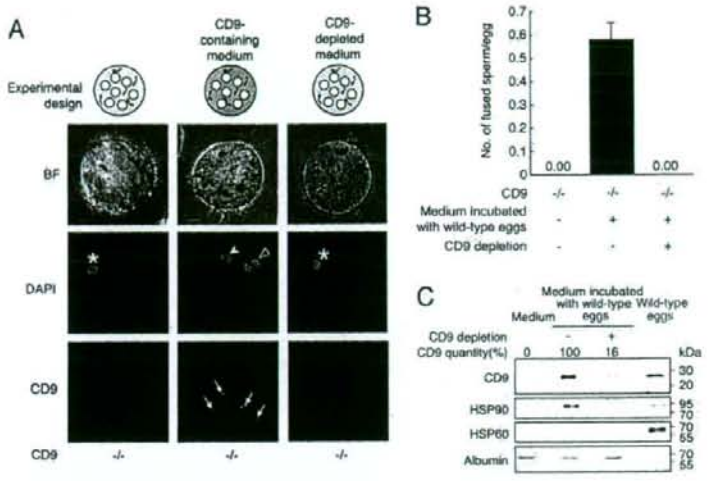

Fig. 4. Identification of fusion-facilitating activity of CD9-containing vesicles. (*A*) Estimation of the fusion-facilitating ability of the vesicles in sperm–egg fusion. As shown in the experimental design, $CD9^{-/-}$ sperm were incubated with $CD9^{-/-}$ eggs (white circles) in media containing egg-released vesicles after the zona pellucida was removed from these eggs. CD9 was detected by anti-CD9 mAb conjugated with Alexa488. The eggs were preloaded with DAPI before incubation with the sperm, to allow counting of the number of fused sperm. (*Left*) $CD9^{-/-}$ eggs at 1 h after incubation with the sperm, as a negative control. *Center* $CD9^{-/-}$ eggs cultured in the medium containing CD9 collected from wild-type eggs. (*Right*) $CD9^{-/-}$ eggs cultured in the medium depleted of CD9 by beads conjugated with anti-CD9 mAb, showing the fused sperm to eggs (arrowhead), metaphase II–arrested chromosomes (*), a second polar body (open arrowhead), and CD9 translocated on the sperm heads (arrow). The fluorescent z-series images were projected as three-dimensional images. Scale bar: 20 μm. (*B*) Number of fused sperm with the zona-free eggs counted at 1 h after incubation (mean ± SEM): $CD9^{-/-}$ eggs as a negative control ($n = 51$), $CD9^{-/-}$ eggs cultured in the medium containing CD9 ($n = 112$), and $CD9^{-/-}$ eggs cultured in the medium depleted of CD9 by antibody-conjugated beads ($n = 74$). The total numbers of eggs examined are in parentheses. (*C*) Western blot analysis of the media incubated with $CD9^{+/+}$ eggs for CD9, HSP90, and HSP60. Loaded samples (left to right): The medium as a negative control, the medium containing the remnant material from 40 eggs per lane (bead-untreated and -treated), and 5 eggs per lane as a positive control. The albumin contained in the medium was detected by Coomassie brilliant blue staining as an internal control. The quantities of CD9 in the media were measured densitometrically (using National Institutes of Health Image software).

that the decreased amount of CD9 after the bead treatment was synchronized with that of a cytoplasmic chaperone, HSP90 (17), but not with a mitochondrial chaperone, HSP60 (18). Our analysis of the egg-conditioned medium indicated that CD9-containing vesicles contained HSP90, a conserved component of exosomes (9, 10).

To estimate the contribution of CD9-containing vesicles to sperm–egg fusion, we examined the restoration of the impaired sperm-fusing ability in $CD9^{-/-}$ eggs co-incubated with $CD9^{+/-}$ or $CD9^{+/+}$ eggs expressing endogenous CD9 (Figs. 5 and S4*A*). We predicted that when sperm were incubated with a mixture of eggs, the vesicles released from $CD9^{+/-}$ or $CD9^{+/+}$ eggs would

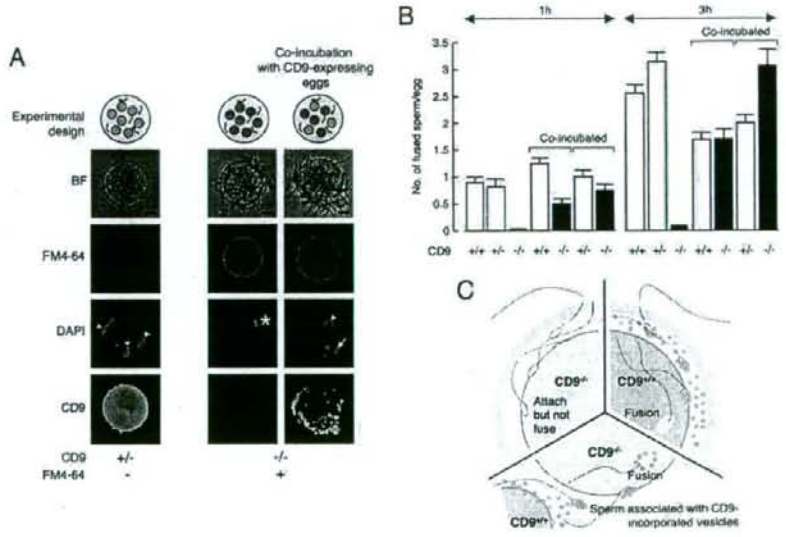

Fig. 5. Recovery of impaired fusion of $CD9^{-/-}$ eggs with sperm by CD9-containing vesicles. (*A*) Estimation of the fusion-facilitating ability of the vesicles in sperm–egg fusion. As shown in the experimental design, sperm were incubated with a mixture of CD9-expressing eggs (green circles) and $CD9^{-/-}$ eggs (red circles) after the zona pellucida was removed from these eggs. The eggs were preloaded with DAPI before incubation with sperm, to allow counting of the number of fused sperm. $CD9^{-/-}$ eggs were prestained with FM4–64 and thus were easily distinguished from CD9-expressing eggs after incubation with the sperm. (*Left*) $CD9^{+/-}$ eggs at 1 h after incubation with the sperm, as a positive control. (*Center*) $CD9^{-/-}$ eggs, as a negative control. (*Right*) $CD9^{-/-}$ eggs co-incubated with $CD9^{+/-}$ eggs, showing fused sperm to egg (arrowheads), metaphase II–arrested chromosomes (*), and extruded second polar body (arrow). The fluorescent z-series images were projected as three-dimensional images. CD9 was detected by anti-CD9 mAb conjugated with Alexa488. Scale bar: 20 μm. (*B*) Numbers of fused sperm with the zona-free eggs counted at 1 and 3 h after incubation (mean ± SEM). $CD9^{+/-}$ (1 h: $n = 34$; 3 h: $n = 55$), $CD9^{+/+}$ (1 h: $n = 71$; 3 h: $n = 79$), and $CD9^{-/-}$ eggs (1 h: $n = 100$; 3 h: $n = 115$) were separately incubated with sperm. Total number of coincubated eggs examined: $CD9^{+/-}$ eggs ($n = 54$) coincubated with $CD9^{-/-}$ eggs ($n = 60$), and $CD9^{+/+}$ eggs ($n = 65$) coincubated with $CD9^{-/-}$ eggs ($n = 74$) at 1 h; $CD9^{+/-}$ eggs ($n = 51$) coincubated with $CD9^{-/-}$ eggs ($n = 33$), and $CD9^{+/+}$ eggs ($n = 98$) coincubated with $CD9^{-/-}$ eggs ($n = 90$) at 3 h. (*C*) Schematic model of involvement of CD9-containing vesicles in sperm–egg fusion: $CD9^{+/+}$ (green), $CD9^{-/-}$ (light blue), and $CD9^{-/-}$ eggs coincubated with $CD9^{+/+}$ wild-type eggs with sperm (yellow).

interact with sperm, and these sperm could fuse with $CD9^{-/-}$ eggs. If sperm-fusing ability were regulated mainly by CD9-containing vesicles, then the number of sperm fused to $CD9^{-/-}$ eggs would be predicted to be almost equal to that fused to $CD9^{+/-}$ or $CD9^{+/+}$ eggs coincubated with $CD9^{-/-}$ eggs. We counted the number of fused sperm in coincubated CD9-expressing eggs ($CD9^{+/-}$ and $CD9^{+/+}$) and $CD9^{-/-}$ eggs. The $CD9^{-/-}$ eggs were prestained with FM4–64 (19), a fluorescent dye used to stain the membrane of live cells, and thus could be easily distinguished from the $CD9^{+/-}$ and $CD9^{+/+}$ eggs. FM4–64 did not transfer between the $CD9^{-/-}$ eggs and the $CD9^{+/-}$ or $CD9^{+/+}$ eggs. As shown in the experimental design, after the zona pellucida was removed from the eggs, $CD9^{-/-}$ eggs (red circles) were mixed with $CD9^{+/-}$ or $CD9^{+/+}$ eggs (green circles), and sperm were added to the medium containing these eggs (Fig. 5*A*). At 1 h after insemination, significant fusion of sperm with the $CD9^{-/-}$ eggs was facilitated (0.75 ± 0.11 and 0.50 ± 0.09 sperm fused per egg), corresponding to that in the $CD9^{+/-}$ (1.00 ± 0.13) and $CD9^{+/+}$ eggs (1.25 ± 0.10). At 3 h after insemination, the fusion of sperm with the $CD9^{-/-}$ eggs was restored (3.06 ± 0.30 and 1.70 ± 0.18 sperm fused per egg) to levels comparable to those in the $CD9^{+/-}$ (2.00 ± 0.15) and $CD9^{+/+}$ eggs (1.69 ± 0.13). We also detected a second polar body extruding from the $CD9^{-/-}$ eggs (Fig. 5*A Right*, arrow). In contrast, we did not observe the translocation of vesicles from the $CD9^{+/-}$ and $CD9^{+/+}$ eggs to the $CD9^{-/-}$ eggs when sperm were not added to the mixture, even after 10 h of incubation (Fig. S4*B*). These data demonstrate that the defect in the fusing ability of $CD9^{-/-}$ eggs is caused by dysfunction of the mechanism facilitating the sperm-fusing activity through CD9-containing vesicles.

To further study the involvement of CD9-containing vesicles in regulating sperm-fusing ability, we evaluated the capability of hamster eggs in sperm–egg fusion (Fig. S5). Hamster eggs have the ability to fuse with other mammalian sperm and thus are used as a tool to evaluate the fusing ability of human sperm (20). When hamster eggs were incubated with $CD9^{-/-}$ eggs after the zona pellucida was removed from these eggs, the sperm-fusing ability of these eggs was improved significantly. The sperm-fusing ability acquired through the exposure to hamster eggs was not as great as that produced by exposure to mouse eggs, probably due to the slightly different CD9 in hamster and mouse eggs (21). These results indicate that the function of CD9-containing vesicles in the acquisition of sperm-fusing ability is widely conserved in mammals.

Discussion

In sperm–egg fusion, there is a significant direct interaction between the cell membranes of sperm and eggs (1, 20, 22); however, our results demonstrate that CD9-containing vesicle–sperm interaction precedes the direct cell membrane interaction between sperm and eggs. Based on our data, we propose that the release of CD9-containing vesicles from eggs before fertilization facilitates the sperm-fusing ability that renders the sperm competent to fuse with $CD9^{-/-}$ eggs (Fig. 5*C*). Our finding of CD9-EGFP in living unfertilized eggs demonstrates that CD9-containing vesicles are present in the PVS, and that these vesicles accumulate inside the PVS during the germinal vesicle (1) and metaphase II-arrested stages (1). During this period, the egg undergoes drastic cytological changes with the increased number of microvilli (1, 22), predicting the correlation between vesicle release and microvilli formation. As expected, this correlation is supported by the finding that CD9 deficiency leads not only to impaired microvilli formation (8) (Fig. S2), but also to decreased accumulation of vesicles within the PVS. These data support the association between the release of CD9-containing vesicles from eggs and the formation of microvilli on the egg plasma membrane.

As reported previously, somatic cells are capable of releasing proteins and lipids included in membrane organelles, termed exosomes (9, 10), which are pinched out from the plasma membrane (23). Exosomes share many additional properties with retroviral particles, including similar lipid and protein compositions, such as tetraspanin (23). GM3 and HSP90 are known to be conserved components of exosomes (10). Our results show that CD9-containing vesicles released from eggs share these two components, implying that the vesicles are "exosome-like." Previous studies of macrophages have proposed that exosome biogenesis occurs only by outward budding at endosomal membranes, followed by the fusion of vesicle-laden endosomes with the plasma membrane (9, 23). If the CD9-containing vesicle were derived from exosomes and generated from the fusion of endosomes with the plasma membrane, then the vesicles would contain some proteases (9, 23), fuse with the sperm membrane, and possibly activate the sperm fusogenic factor(s) by enzymatic activities.

In hamster eggs, expansion of the PVS has been deemed essential or at least beneficial to normal fertilization (20, 21, 24), indicating that materials involved in fusion with sperm are released from eggs before fertilization in hamsters and in mice. Because anti-CD9 mAbs are not available for hamster CD9, we could not directly confirm CD9-containing vesicle release from hamster eggs before fertilization. Instead, our co-incubation assay demonstrated that hamster eggs facilitate the fusion of sperm with $CD9^{-/-}$ eggs, indicating that hamster eggs share a similar mechanism with mouse eggs through egg-released materials. Moreover, it has been reported that growing oocytes bind to sperm and transfer fluorescent dyes to the sperm head (25). At this stage, oocytes have CD9 on the cell membrane but lack CD9-containing vesicles (Fig. S1). We presume that the transfer of fluorescent dye from growing oocytes to sperm heads is mediated by CD9 on the cell membrane. Based on our findings, we propose that the CD9-containing vesicle has an ability to facilitate sperm—egg fusion. This knowledge has great potential for clinical applications, such as the induction of sperm–egg fusion using exogenous sources.

Materials and Methods

Animals. The mice that we produced were back-crossed into a C57BL/6 genetic background. Wild-type eggs were collected from C57BL/6 females (8–12 weeks old). Wild-type sperm were obtained from the epididymides of B6C3F1 males (8–12 weeks old). Hamster eggs were obtained commercially as frozen unfertilized eggs (NOSAN).

Antibodies and Chemicals. Antibodies against CD9 (KMC; BD PharMingen), beta-tubulin (Tub2.1; Sigma), HSP60 (24/HSP60; BD PharMingen), HSP90 (16F1; MBL), and GM3 (GMR6; Seikagaku) were used. Antibodies labeled with biotin by a labeling kit (Dojindo) and horseradish peroxidase-conjugated streptavidin (Sigma) were used for Western blot analysis. For immunostaining, antibodies were labeled directly with Alexa488 and Alexa546 using labeling kits (Invitrogen). FM4–64 (Invitrogen) was used to define the lipid bilayer of live eggs without disturbing sperm–egg fusion (10 μM at final concentration). We used DAPI (Invitrogen), a fluorescent dye that slowly permeates the living cell membrane (semipermeable) and slowly leaks out of cells after washing relative to Hoechst33342 (permeable), in counting the number of sperm fused per egg.

Transgenic Mice. The construct expressing mouse CD9 tagged at the N terminus with EGFP (CD9-EGFP) was subcloned into plasmid DNA-containing mouse ZP3 promoter (26). The expression cassette was excised by restriction enzyme digestion and microinjected into fertilized eggs of C57BL/6 mice, according to standard techniques (27).

Genotyping and RT-PCR. Mouse genotyping and RT-PCR were performed following standard procedures (27). (Primer sets are listed in Table S1).

Egg Collection. Eggs were collected from the oviduct 14–16 h after human chorionic gonadotropin injection (4). The eggs were placed in a drop of TYH

medium (28). Sperm collected from the epididymides were capacitated in a 100-μl drop of medium. The eggs were incubated with 1.5×10^5 sperm/ml at 37°C in 5% CO_2, and unbound sperm were washed away. The zona pellucida was removed from the eggs with acidic Tyrode's solution (4) or a piezo manipulator (11). A hole was punched through the zona pellucida with a piezo manipulator, and the eggs were removed. All materials were aspirated, including the medium but not the eggs, and used as "remnants."

Immunostaining. Zona-intact live eggs were stained with diluted antibodies in TYH medium for 30 min at 37°C, and the nonspecifically accumulated antibodies in the PVS were washed away after a brief incubation (30 min) in the medium. To measure the fluorescent intensities of GM3, three types of eggs were stained by Alexa546-labeled anti-GM3 mAb in TYH medium for 30 min, then washed in the medium for 30 min. Staining was visualized using a laser scanning confocal microscope (LSM 510 META; Carl Zeiss).

Electron-Microscopic Analysis. Live eggs were incubated with anti-CD9 mAb and anti-rat IgG mAb tagged with 5-nm gold beads. After incubation, the eggs were fixed by glutaraldehyde and osmic acid solutions. Ultra-thin sections were prepared as described in ref. 29. Eggs denuded with acid Tyrode's solution were fixed with a mixture of paraformaldehyde and glutaraldehyde and osmic acid solutions.

***In Vitro* Fertilization.** To observe the fusion with the sperm, zona-intact and zona-free eggs were incubated with DAPI (10 μg/ml) in the medium for 20 min, then washed before the sperm were added. This procedure allowed the staining of only fused sperm nuclei by dye-transfer into sperm after membrane fusion. At 1 h or 3 h after incubation in a 30-μl drop of medium, the eggs were fixed with a mixture of paraformaldehyde and glutaraldehyde for 20 min at 4°C.

Monitoring the Association of CD9-Containing Vesicles with Sperm. Eggs collected from Tg$^+$CD9$^{-/-}$ females were set in a 30-μl drop of TYM medium. The sperm were added to the eggs at a final concentration of 1.5×10^5/ml after incubation in the medium for 2 h. Posts of latex beads were deposited around the eggs. A glass coverslip was carefully pressed down onto the posts until the egg were fixed. The medium containing eggs and sperm was cooled to 10°C before observation. Cooling reduced the sperm motility. This procedure allowed us to measure the CD9-EGFP fluorescence on the sperm head using a confocal microscope. Images of the sperm were captured at 1 frame/s. The average value of the fluorescent intensities of CD9-EGFP at 0 s was set to 100%, and the final concentration of antibodies was adjusted to 50 μg/ml. The data are measurements of serial images from 15 wild-type sperm in triplicate dishes.

Collection of CD9-Containing Vesicles. The medium containing the vesicles was collected from denuded wild-type eggs. The eggs were cultured in a 60-μl drop of medium for 2 h after the zona pellucida was removed from the eggs. Collecting the medium containing the vesicles required an incubation time of 2 h. The collected medium was used for analysis of vesicle components and evaluation of sperm-fusing ability. CD9-depleted medium was used as a negative control. After the zona pellucida was removed from CD9$^{-/-}$ eggs, the eggs were incubated with the sperm in the medium containing CD9-incorporated vesicles for 1 h, for comparison with the vesicle-depleted medium. Details are shown in Fig. S3.

Western Blot Analysis. Quantities of proteins were examined by Western blot analysis, as described in ref. 4. As an internal loading control, quantities of albumin included in the medium were examined using Coomassie brilliant blue staining. Details are shown in Fig. S3.

Coincubation of Two Types of Eggs. CD9$^{-/-}$ eggs and CD9-expressing eggs (CD9$^{+/-}$ and CD9$^{+/+}$) were incubated in each 30-μl drop of medium after the zona pellucida was removed from these eggs. At 2 h after incubation, the CD9$^{-/-}$ eggs were added into the cultured medium of the CD9-expressing eggs. Sperm were added into the medium containing two types of eggs and incubated for 1 or 3 h. Details are shown in Fig. S4A. The frozen hamster eggs also were incubated with the CD9$^{-/-}$ eggs and wild-type sperm for 1 h. The zona pellucida of frozen hamster eggs was hardened, and removing the zona pellucida using acid Tyrode's solution took 5 min. Details are shown in Fig. S5A.

ACKNOWLEDGMENTS. This work was supported by a Precursory Research for Embryonic Science and Technology (PRESTO) grant from the Japanese Ministry of Health, Labor and Welfare and by a Grant-in-Aid for Scientific Research from the Japanese Ministry of Education, Culture, Sports, and Technology.

1. Yanagimachi R (1994) in *The Physiology of Reproduction*, eds Knobil E, Neill JD (Raven, New York), pp 189–317.
2. Kaji K, *et al.* (2000) The gamete fusion process is defective in eggs of Cd9-deficient mice. *Nat Genet* 24:279–282.
3. Le Naour F, Rubinstein E, Jasmin C, Prenant M, Boucheix C (2000) Severely reduced female fertility in CD9-deficient mice. *Science* 287:319–321.
4. Miyado K, *et al.* (2000) Requirement of CD9 on the egg plasma membrane for fertilization. *Science* 287:321–324.
5. Hemler ME (2003) Tetraspanin proteins mediate cellular penetration, invasion, and fusion events and define a novel type of membrane microdomain. *Annu Rev Cell Dev Biol* 19:397–422.
6. Barraud-Lange V, Naud-Barriant N, Bomsel M, Wolf J-P, Ziyyat A (2007) Transfer of oocyte membrane fragments to fertilizing spermatozoa. *FASEB J* 21:3446–3449.
7. Joly E, Hudrisier D (2003) What is trogocytosis and what is its purpose? *Nat Immunol* 4:815.
8. Runge K-E, *et al.* (2007) Oocyte CD9 is enriched on the microvillar membrane and required for normal microvillar shape and distribution. *Dev Biol* 304:317–325.
9. Trajkovic K, *et al.* (2008) Ceramide triggers budding of exosome vesicles into multivesicular endosomes. *Science* 319:1244–1247.
10. Wubbolts R, *et al.* (2003) Proteomic and biochemical analyses of human B cell-derived exosomes: Potential implications for their function and multivesicular body formation. *J Biol Chem* 278:10963–10972.
11. Yamagata K, *et al.* (2002) Sperm from the calmegin-deficient mouse have normal abilities for binding and fusion to the egg plasma membrane. *Dev Biol* 250:348–357.
12. Mitsuzuka K, Handa K, Satoh M, Arai Y, Hakomori S (2005) A specific microdomain ("glycosynapse 3") controls phenotypic conversion and reversion of bladder cancer cells through GM3-mediated interaction of alpha3beta1 integrin with CD9. *J Biol Chem* 280:35545–35553.
13. Yamashita T, *et al.* (2003) Enhanced insulin sensitivity in mice lacking ganglioside GM3. *Proc Natl Acad Sci USA* 100:3445–3449.
14. Kotani M, Ozawa H, Kawashima I, Ando S, Tai T (1992) Generation of one set of monoclonal antibodies specific for a-pathway ganglio-series gangliosides. *Biochim Biophys Acta* 1117:97–103.
15. Chen MS, *et al.* (1999) Role of the integrin-associated protein CD9 in binding between sperm ADAM 2 and the egg integrin alpha6beta1: Implications for murine fertilization. *Proc Natl Acad Sci USA* 96:11830–11835.
16. Miller B-J, Georges-Labouesse E, Primakoff P, Myles D-G (2000) Normal fertilization occurs with eggs lacking the integrin alpha6beta1 and is CD9-dependent. *J Cell Biol* 149:1289–1296.
17. Callahan M-K, Garg M, Srivastava P-K (2008) Heat-shock protein 90 associates with N-terminal extended peptides and is required for direct and indirect antigen presentation. *Proc Natl Acad Sci USA* 105:1662–1667.
18. Cheng M-Y, Hartl F-U, Horwich A-L (1990) The mitochondrial chaperonin hsp60 is required for its own assembly. *Nature* 348:455–458.
19. Bolte S, *et al.* (2004) FM-dyes as experimental probes for dissecting vesicle trafficking in living plant cells. *J Microsc* 214:159–173.
20. Yanagimachi R, Yanagimachi H, Rogers B-J (1976) The use of zona-free animal ova as a test system for the assessment of the fertilizing capacity of human spermatozoa. *Biol Reprod* 15:471–476.
21. Ponce R-H, Yanagimachi R, Urch U-A, Yamagata T, Ito M (1993) Retention of hamster oolemma fusibility with spermatozoa after various enzyme treatments: A search for the molecules involved in sperm–egg fusion. *Zygote* 1:163–171.
22. Primakoff P, Myles D-G (2002) Penetration, adhesion, and fusion in mammalian sperm–egg interaction. *Science* 296:2183–2185.
23. Booth A-M, *et al.* (2006) Exosomes and HIV Gag bud from endosome-like domains of the T cell plasma membrane. *J Cell Biol* 172:923–935.
24. Okada A, Yanagimachi R, Yanagimachi H (1986) Development of a cortical granule-free area of cortex and the perivitelline space in the hamster oocyte during maturation and following ovulation. *J Submicrosc Cytol* 18:233–247.
25. Zuccotti M, Yanagimachi R, Yanagimachi H (1991) The ability of hamster oolemma to fuse with spermatozoa: Its acquisition during oogenesis and loss after fertilization. *Development* 112:143–152.
26. Rankin T-L, *et al.* (1998) Human ZP3 restores fertility in Zp3 null mice without affecting order-specific sperm binding. *Development* 125:2415–2424.
27. Hogan B, Costantini F, Lacy E (1986) in *Manipulating the Mouse Embryo* (Cold Spring Harbor Lab Press, Cold Spring Harbor, NY), pp 217–252.
28. Toyoda Y, Chang M-C (1974) Capacitation of epididymal spermatozoa in a medium with high K-Na ratio and cyclic AMP for the fertilization of rat eggs in vitro. *J Reprod Fertil* 36:125–134.
29. Toshimori K, Saxena D-K, Tanii I, Yoshinaga K (1998) An MN9 antigenic molecule, equatorin, is required for successful sperm–oocyte fusion in mice. *Biol Reprod* 59:22–29.